



# Simulated Tip Rub Testing of Low-Density Metal Foam

*Cheryl L. Bowman  
Glenn Research Center, Cleveland, Ohio*

*Michael G. Jones  
Langley Research Center, Hampton, Virginia*

## NASA STI Program . . . in Profile

Since its founding, NASA has been dedicated to the advancement of aeronautics and space science. The NASA Scientific and Technical Information (STI) program plays a key part in helping NASA maintain this important role.

The NASA STI Program operates under the auspices of the Agency Chief Information Officer. It collects, organizes, provides for archiving, and disseminates NASA's STI. The NASA STI program provides access to the NASA Aeronautics and Space Database and its public interface, the NASA Technical Reports Server, thus providing one of the largest collections of aeronautical and space science STI in the world. Results are published in both non-NASA channels and by NASA in the NASA STI Report Series, which includes the following report types:

- **TECHNICAL PUBLICATION.** Reports of completed research or a major significant phase of research that present the results of NASA programs and include extensive data or theoretical analysis. Includes compilations of significant scientific and technical data and information deemed to be of continuing reference value. NASA counterpart of peer-reviewed formal professional papers but has less stringent limitations on manuscript length and extent of graphic presentations.
- **TECHNICAL MEMORANDUM.** Scientific and technical findings that are preliminary or of specialized interest, e.g., quick release reports, working papers, and bibliographies that contain minimal annotation. Does not contain extensive analysis.
- **CONTRACTOR REPORT.** Scientific and technical findings by NASA-sponsored contractors and grantees.

- **CONFERENCE PUBLICATION.** Collected papers from scientific and technical conferences, symposia, seminars, or other meetings sponsored or cosponsored by NASA.
- **SPECIAL PUBLICATION.** Scientific, technical, or historical information from NASA programs, projects, and missions, often concerned with subjects having substantial public interest.
- **TECHNICAL TRANSLATION.** English-language translations of foreign scientific and technical material pertinent to NASA's mission.

Specialized services also include creating custom thesauri, building customized databases, organizing and publishing research results.

For more information about the NASA STI program, see the following:

- Access the NASA STI program home page at <http://www.sti.nasa.gov>
- E-mail your question via the Internet to [help@sti.nasa.gov](mailto:help@sti.nasa.gov)
- Fax your question to the NASA STI Help Desk at 443-757-5803
- Telephone the NASA STI Help Desk at 443-757-5802
- Write to:  
NASA Center for AeroSpace Information (CASI)  
7115 Standard Drive  
Hanover, MD 21076-1320



# Simulated Tip Rub Testing of Low-Density Metal Foam

*Cheryl L. Bowman  
Glenn Research Center, Cleveland, Ohio*

*Michael G. Jones  
Langley Research Center, Hampton, Virginia*

National Aeronautics and  
Space Administration

Glenn Research Center  
Cleveland, Ohio 44135

## Acknowledgments

The authors would like to acknowledge the foundational work on metallic foams performed by Dr. Mohan Hebsur, formerly of Ohio Aerospace Institute. The tip rub test rig was developed by Jose C. Gonzalez in support of the Rotor Alone Nacelle Phase of the Advanced Subsonic Technology Program. System configuration, controller configuration, and data acquisition system development as well as testing support were provided by Derek Podboy, John DeArmon, and Don Hammett, Jr., of NASA Glenn Research Center, TFOME/Jacobs Sverdrup, and TFOME/Sierra Lobo, respectively. Acoustic impedance tests were conducted by Carol Harrison of NASA Langley Research Center.

Trade names and trademarks are used in this report for identification only. Their usage does not constitute an official endorsement, either expressed or implied, by the National Aeronautics and Space Administration.

This work was sponsored by the Fundamental Aeronautics Program at the NASA Glenn Research Center.

*Level of Review:* This material has been technically reviewed by technical management.

Available from

NASA Center for Aerospace Information  
7115 Standard Drive  
Hanover, MD 21076-1320

National Technical Information Service  
5285 Port Royal Road  
Springfield, VA 22161

Available electronically at <http://gltrs.grc.nasa.gov>

# Simulated Tip Rub Testing of Low-Density Metal Foam

Cheryl L. Bowman  
National Aeronautics and Space Administration  
Glenn Research Center  
Cleveland, Ohio 44135

Michael G. Jones  
National Aeronautics and Space Administration  
Langley Research Center  
Hampton, Virginia 23681

## Abstract

Preliminary acoustic studies have indicated that low-density, open-cell, metal foams may be suitable acoustic liner material for noise suppression in high by-pass engines. Metal foam response under simulated tip rub conditions was studied to assess whether its durability would be sufficient for the foam to serve both as a rub strip above the rotor as well as an acoustic treatment. Samples represented four metal alloys, nominal cell dimensions ranging from 60 to 120 cells per inch (cpi), and relative densities ranging from 3.4 to 10 percent. The resulting rubbed surfaces were relatively smooth and the open cell structure of the foam was not adversely affected. Sample relative density appeared to have significant influence on the forces induced by the rub event. Acoustic responses of various surface preparations were measured using a normal incidence tube. The results of this study indicate that the foam's open-cell structure was retained after rubbing and that the acoustic absorption spectra variation was minimal.

## Introduction

Open-cell, porous metals are used most commonly in battery electrodes, biomedical applications filtration systems, certain heat exchanger functions, and a variety of specialty applications (Ref. 1). Low-density metal foams are currently being explored for possible incorporation as a multifunctional component in an advanced turbine engine case. Metal foams have several characteristics that could be used in a sophisticated engine case design. Low-density foams have useful impact-absorption behavior because the local deformation is unconstrained by the surrounding material, unlike solid materials in which indentation plasticity is constrained by surrounding material. This unconstrained deformation can result in a stress-strain plateau that leads to good energy absorption. Sandwich panels traditionally are high stiffness-to-density structures and metal foams are a viable candidate for sandwich materials at warm to high temperatures. Perhaps the most enticing characteristic is that open cell foams can dissipate sound energy and therefore offer potential as acoustic treatment in an engine case. Previous testing in a low-speed, ducted fan test rig indicated potential noise reduction benefits by locating metal foam liners fore, aft, and over a fan rotor (Ref. 2). Some of the most promising acoustic absorption results were obtained with the metal foam was placed over the rotor or just in front of the rotor. If placed over the rotor, the foam would be vulnerable to damage caused by the tips of the fan blades. A rub event potentially could smear and effectively close the foam surface. Or damage to the foam surface could propagate and cause generalized loss of material. This paper summarizes testing which addressed the physical response of metal foam to simulated tip rub conditions.

## Nomenclature

spi	Cells per inch
OASPL	Overall sound pressure level
PACS	Probe Actuator Control System
PV	Percent variability
$\alpha$	Frequency-dependent absorption coefficient
$\theta$	Normalized, frequency-dependent acoustic resistance
$\chi$	Normalized, frequency-dependent acoustic reactance

## Materials

The metal foams in this study were produced by Porvair Advanced Materials/Selee Corporation Hendersonville, North Carolina. These porous materials are formed by a metal sintering process where metallic particles are suspended in slurry and coated over an open-cell polymeric foam template. The polymeric foam skeleton vaporizes during heat treatment and the metallic particles sinter in its place. Lefebvre (Ref. 1) reserves the term metal foam for materials formed by a foaming process, but the term metal foam is used here due to the way the metal closely follows the structure of the foam template. This processing technique produces an open-cell structure that has a high degree of variation. Within-ligament porosity is prevalent because the metal does not fill the space of the original polymeric foam skeleton. The cell ligaments have varying thickness and it is common to find cell walls. The advantages of this processing technique include its ability to produce a wide range of alloy types, cell sizes, and relative densities. Moreover, this approach appears to be capable of near-net-shape production of parts suitable for fan case application. The flexibility of this processing route makes it attractive for the design of multifunctional components and especially useful for surveying variable responses as a function of alloy type, nominal cell size, and relative density.

The foams studied here were made from the four different alloys listed below with nominal chemistry given in weight percent.

- Haynes 25: Co-51, Ni-10, Cr-20, W-15, Fe-3max, Mn-1.5, Si-0.4max, C-0.10
- FeCrAlY: Fe-73, Cr-22, Al-5, Y-trace
- 316 stainless steel: Fe-66, Cr-17, Ni-12, Mo-2, Mn-2, Si-1, C-0.1, P-0.04, S-0.03
- 314 stainless steel: Fe-52, Cr-24, Ni-20, Mn-2, Si-2, C-0.2, P-0.04, S-0.03

Haynes 25 (Haynes International Inc.) was selected because previous research has shown that it has very good specific impact resistance as well as oxidation resistance that would allow application in hotter sections of the engine (Ref. 3). FeCrAlY, also known as Fecralloy (AEA Technology, Harwell) or Kanthal (Kanthal Group companies), is an iron alloy that has good corrosion/oxidation resistance and is a common heat exchanger product. The 316 and 314 stainless steels are austenitic alloys with good corrosion resistance.

The cell size of an irregularly shaped foam network can be measured in several ways. The linear density of cells (cells per inch) is one convenient expression of cell size but it would not give the same value as a statistical average of cell diameters. The cell size of these foams were reported by the manufacturer as “pores per inch”. In-house measurements have found that the cell distribution as determined by counting cells (a.k.a. pores) along a linear dimension was finer than that reported by the manufacturer (higher number of cells per inch). It is possible that the manufacturer values were based on the pores per inch of the template foam and that the higher measured values are due to shrinkage during sintering. For simplicity, the manufacturer’s reported cell size will be used in this report. Therefore care must be exercised when comparing the results of this report with foams produced by other manufacturing

techniques. The term “cells per inch” (cpi) will be used to distinguish the macroscopic cell architecture from the finer pores found within the cell ligaments.

The relative density is the density of the porous material normalized by the parent alloy density. Foams with relative densities from 3 to 10 percent were used in this study. The average relative densities measured in-house agreed well with those reported by the manufacturer. However, in-house measurements have found that localized density variations of 0.5 percent relative density are not uncommon. That is, the average relative density of 1 cm cubes from the same parent panel might be 6.1 percent and the measured values fall between 6.9 and 5.6 percent.

## Simulated Tip Rub Testing

### Tip Rub Sample Materials

Metal foam samples were selected to screen the rub response as a function of alloy type, cell size, and relative density. Table I summarizes the foam materials tested. The sample identification nomenclature includes reference to the alloy type, cells per inch, and an alphanumeric panel designation. In the sample identification nomenclature, FEC is FeCrAlY, HAY is Haynes 25, SS314 is 314 stainless steel, and SS316 is 316 stainless steel. Rectangular 127 by 38 mm (5 by 1.5 in.) samples were cut from the panels using a band saw. In general, only one rub test was performed per sample. Repeat tests, designated by (r) in Table I, were performed on three samples by flipping the sample axial in the specimen holder. The cell size and relative density values listed in Table I are those provided by the manufacturer; these are nominal values that must be applied with caution, as discussed in the previous section. The panels available for making rub samples had different initial thicknesses. This difference in sample thickness was considered to be an insignificant factor in the rub testing.

TABLE I.—FOAM SAMPLES USED IN RUB TESTING  
 [Alloys used were FeCrAlY (FEC), Haynes 25 (HAY), and stainless steel (SS314 or SS316).  
 Cell size (cells per inch) and relative density values are as provided by manufacturer.]

Alloy/ID	Cell per inch, cpi	Panel relative density, percent	Thickness, mm
HAY-80-E	80	4.6	12.7
HAY-80-G	80	6.4	25.4
HAY-100-F	100	6.5	12.7
SS316-60-B(r)	60	5.3	12.7
SS314-80-C(r)	80	4.0	8.9
SS316-80-D	80	5.3	6.4
SS316-120-H	120	5.2	6.1
FEC-60-607xviii	60	4.7	12.5
FEC-60-B	60	5.3	10.2
FEC-60-607Axvi	60	9.7	12.5
FEC-80-C	80	2.9	6.6
FEC-80-D(r)	80	4.0	8.9
FEC-80-607Bxv	80	4.8	12.5
FEC-80-E	80	5.5	25.4
FEC-80-607Di	80	10.0	12.5
FEC-120-807Div	120	4.7	12.5

## Tip Rub Experimental Procedures

The tip rub test was performed on an apparatus designed to simulate the rubbing of blade tips against the surrounding wall material (Ref. 4). The features of this test rig included

- Two-component load balance for measuring radial and tangential loads in the rub strip
- Controlled, variable rotor speeds
- Real-time control of the linear velocity of the sample rub strip material as it contacted the rotating disk teeth

The rotating portion of the test system consisted of a commercially available router motor, a high speed spindle, and a rotor disk with twelve Ti-6Al-4V teeth. The rotor assembly balance was monitored using two accelerometers mounted on the spindle housing. The rotor disk was designed such that the teeth are replaceable and thus other blade materials or geometries could be simulated. The rub-material sample was mounted in a two-axis load frame on motorized traverse structure that provides a controlled insertion into the rotor plane. The load frame was a set of three plates that were sandwiched together with low-friction miniature slides. The slides were configured so that the top plate could freely move in two-dimensions while the bottom plate remained fixed. Two load cells were attached to the middle plate. These load cells were configured to measure force perpendicular to each other. The top and bottom plates were then connected to the appropriate load cells to create a two-component load balance that measured  $x$  and  $y$  loads in the sample corresponding to the tangential and radial directions with respect to the rotor. Three combinations of load cells were used in these tests. Initial tests were conducted with load cell capacities of 445 N (100 lbf) in the  $x$  direction and 2224 N (500 lbf) in the  $y$  direction. The second set of tests was conducted with load cells of 44.5 N (10 lbf) and 445 N (100 lbf), and the last tests were conducted with load cells of 44.5 N (10 lbf) in both directions.

The vertical position of the rub strip sample was controlled by a stepper motor and verified by a linear variable displacement transducer. Position commands were sent to the stepper motor using the in-house designed Probe Actuator Control System (PACS) that allowed for independent control of position and traverse speed. Labview (National Instruments Corporation) software was used to collect the load cell, displacement transducer, and tachometer responses of the system.

Rectangular samples were supported in an adjustable depth frame to accommodate a range of specimen thickness. A mounted sample prior to rub testing is shown in Figure 1. The rub tests were performed using a rotational speed of nominally 10,000 revolutions per minute (rpm), which corresponds to a tip speed of 93 m/s (305 ft/s, 3665 in./s) for the 178 mm (7 in.) diameter rotor. The foam sample traversed down along the  $y$ -axis (radial direction relative to rotor) at a traverse rate of 6.4 mm/s (0.25 in./s). One second rub tests were performed resulting in an incursion that was approximately 6.4 mm (0.25 in.) at the deepest point of the arc. An illustration of the sample, rotor, and force directions is shown in Figure 2. The rotor speed was recorded during the rub event in addition to  $x$  and  $y$  forces induced in the foam sample.

## Tip Rub Results

The primary observation for these tests was that all samples wore gracefully with minimal loading induced in the  $x$  and  $y$  directions. The foam cut away smoothly and the foam did not appear to smear or lose its open cell nature. There were no signs of tearing or gouging regardless of whether the specimen thickness was narrower or wider than the 12.7 mm wide rotor tips. Figure 3 shows an example of a thin wall of foam that was left behind as the rotating tips rubbed away adjacent foam. The three repeat tests were performed on specimen edges that were partially or entirely cut with a band saw blade. These three tests were intended to simulate rubbing across a seam. Figure 4 shows the resulting rub surface after rubbing across a saw cut. In each case there was no noticeable gouging or crumbling at the cut edges.

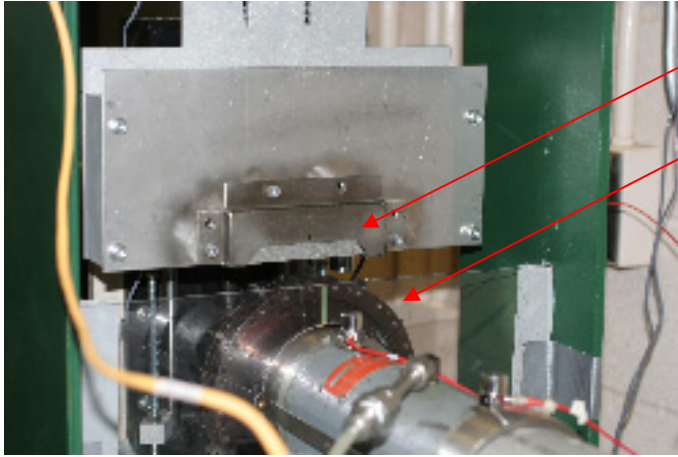


Figure 1.—Metal foam rub sample mounted in two-axis load frame.

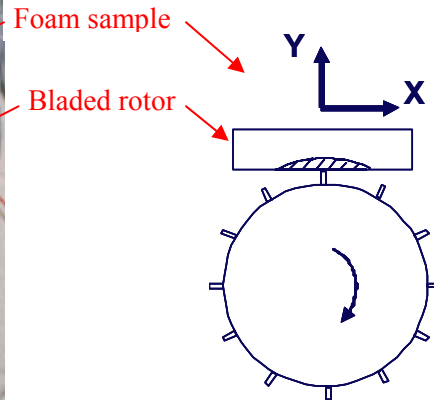


Figure 2.—Illustration of rub test set up. Dashed area indicates area where material is removed.

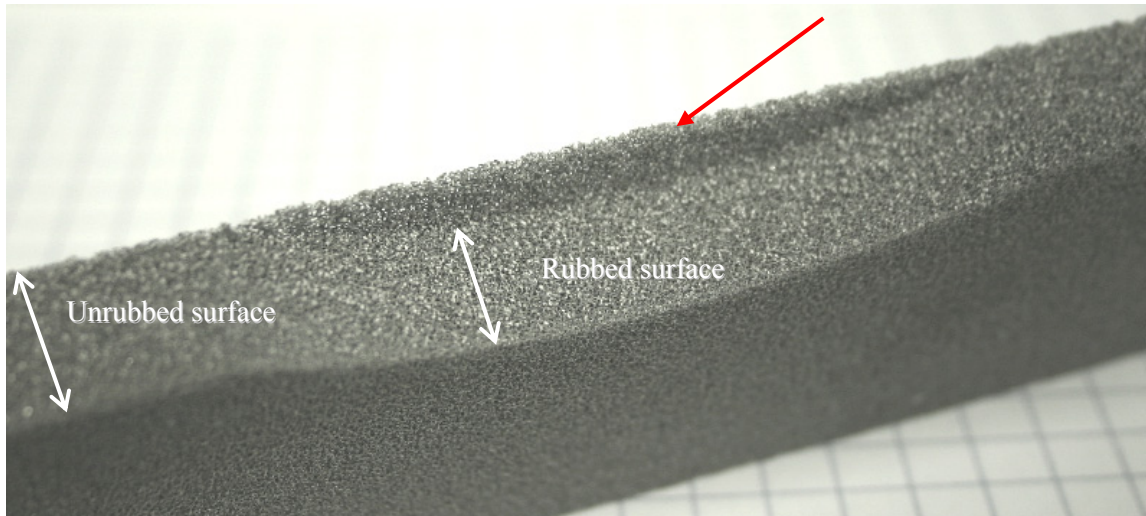


Figure 3.—FEC-80-607Bxv rub specimen showing smooth, semi-circular wear pattern and ~1 mm thick wall of unrubbed foam, indicated with red arrow. The specimen was about the same thickness as the blades were wide, ~12.5 mm. However, the specimen was offset sufficiently to leave a thin section of material unrubbed.



Figure 4.—Repeat rub test on second edge of specimen SS314-80-C. Prior to rub testing a slot was machined in the sample to simulate rubbing over a seam. Remnants of slot visible in center of semi-circular wear pattern. The specimen is 9 mm thick and the rubbed area is approximately 6.3 mm deep.

The forces aligned with the tangential ( $x$ ) direction, radial ( $y$ ) rub direction, and the tachometer responses are summarized in Table II and plotted in Appendix A. An example of the rub-induced loading forces is shown in Figure 5. In most cases, the measured load response was low relative to the overall signal. In order to characterize the change due to the rub event, the average signal before nominal touch (negative position on abscissa) was compared to the average signal in the last 1.3 mm (0.05 in.) of the rub. This increase in average load and decrease in average rotor speed is listed in Table II and with the appendix graphs. Initially, relatively high capacity load cells were used to ensure that load cells would not be damaged. The respective load cell capacities are listed for test sample since the measurement fidelity is best for the tests with the lower capacity load cells. The tachometer readings were not available for five of the rub tests. The three samples that were tested twice, once on each of the 127 mm sample edges, are indicated in Table II with (r) and had similar force and tachometer responses.

TABLE II.—SAMPLE RUB RESPONSE FOR FeCrAlY (FEC), HAYNES 25 (HAY), AND STAINLESS STEEL (SS314 OR SS316) FOAMS IN ASCENDING ORDER OF RELATIVE DENSITY; RELATIVE DENSITY BASED ON RUB SAMPLE MASS AND DIMENSIONS

Alloy/ID	Sample relative density, percent	Load cell	$x$ -force increase, N	$y$ -force increase, N	Speed decrease, rpm
FEC-80-D	3.4	<sup>a</sup> 1	0.5	0.9	21
FEC-80-D(r)	3.4	<sup>c</sup> 3	0.4	0.6	19
FEC-80-C	3.5	1	0.1	1.0	8
SS314-80-C	4.3	<sup>b</sup> 2	0.9	1.0	39
SS314-80-C(r)	4.3	3	0.8	1.1	22
FEC-60-B	4.4	2	0.4	0.5	38
FEC-60-607 <sup>xviii</sup>	4.5	3	1.3	2.2	---
FEC-80-607 <sup>Bxv</sup>	4.6	3	1.3	2.4	---
FEC-80-E	4.8	2	1.5	2.3	65
SS316-60-B	5.0	1	1.0	1.0	54
SS316-60-B(r)	5.0	3	1.8	2.6	74
FEC-120-807 <sup>Div</sup>	5.1	3	0.6	0.5	---
HAY-80-G	5.3	2	1.6	2.9	65
SS316-120-H	5.4	2	0.8	0.3	38
SS316-80-D	5.9	1	1.8	3.0	75
HAY-100-F	6.2	1	4.1	7.9	109
HAY-80-E	6.6	1	4.9	10.4	254
FEC-60-607 <sup>Axvi</sup>	9.5	3	6.8	20.0	---
FEC-80-607 <sup>Di</sup>	9.9	3	9.5	32.3	---

<sup>a</sup>445 N load cell  $x$ -axis, 2224 N load cell  $y$ -axis

<sup>b</sup>44.5 N load cell  $x$ -axis, 445 N load cell  $y$ -axis

<sup>c</sup>44.5 N load cell  $x$ -axis, 44.5 N load cell  $y$ -axis

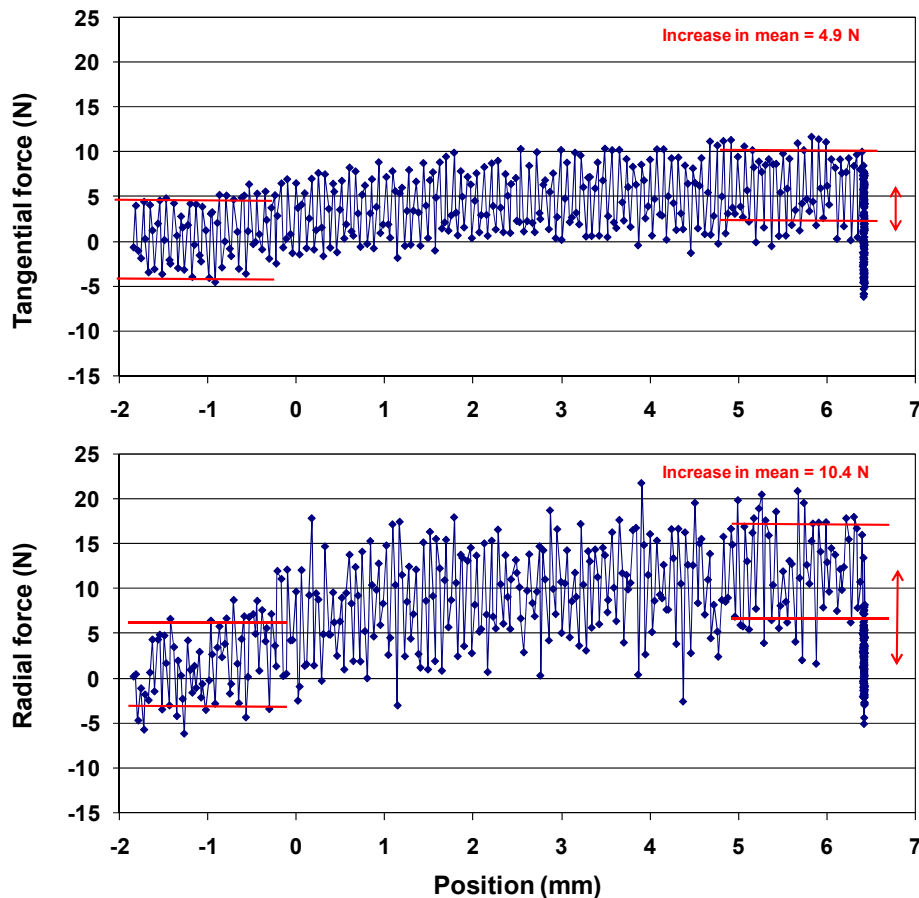


Figure 5.—The tangential (x) and radial (y) rub forces measured on sample HAY-80-E. Red boundary lines illustrate regions for averages of the signal prior to touch and of the final 1.3 mm that were compared to determine the mean force increase. Red arrows indicate magnitude of shift.

In addition to observing the surface damage, the general loading responses were compared based on the alloy type, cell size, and relative density. The relative densities calculated from the measured density of the 127 by 38 mm rub samples were used in analyzing the data rather than that quoted by the manufacturer for the entire panel and it is this sample relative density that is listed in Table II. Figure 6 shows the response of the induced tangential and radial forces with respect to cell size and alloy. There are no discernable trends in these plots. Figure 7 shows the load forces plotted instead as a function of sample relative density. There is a distinct increase in tangential and radial loads as the sample density increases. Table II lists the samples and test results in order of ascending sample relative density. From this data set it appears that relative density is a stronger controlling factor than either cell size or alloy type, but interaction effects certainly cannot be ruled out based on this small sample set.

Figure 8 plots all the FeCrAl alloy tangential (x) and radial (y) rub forces as a function of sample relative density. The filled symbols and the solid regression lines represent the 80 cpi data only. The open symbols include the 60 and 120 cpi samples and the dashed regression lines include all the data. The coefficients of simple determination ( $R^2$  values) are all above 0.9, where 1.0 would be a perfect fit. It is interesting that the regression fits are better if only the 80 cpi data are considered. Also, all the 60 and 120 cpi data points fall below the 80 cpi regression lines. This implies that for a given relative density, the 80 cpi samples have stronger ligaments than the other samples. One possible explanation is that the processing parameters are better optimized for the 80 cpi foam thus producing foams with better ligament integrity and strength.

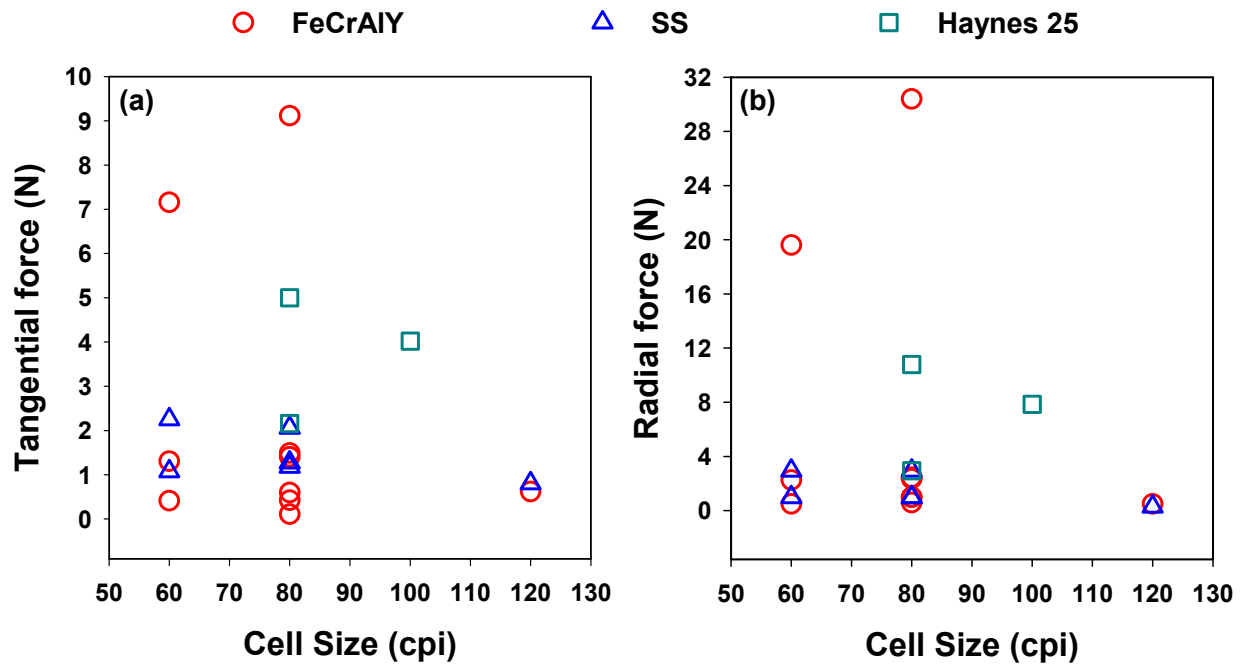


Figure 6.—Rub induced (a) tangential and (b) radial forces as a function of foam cell size.

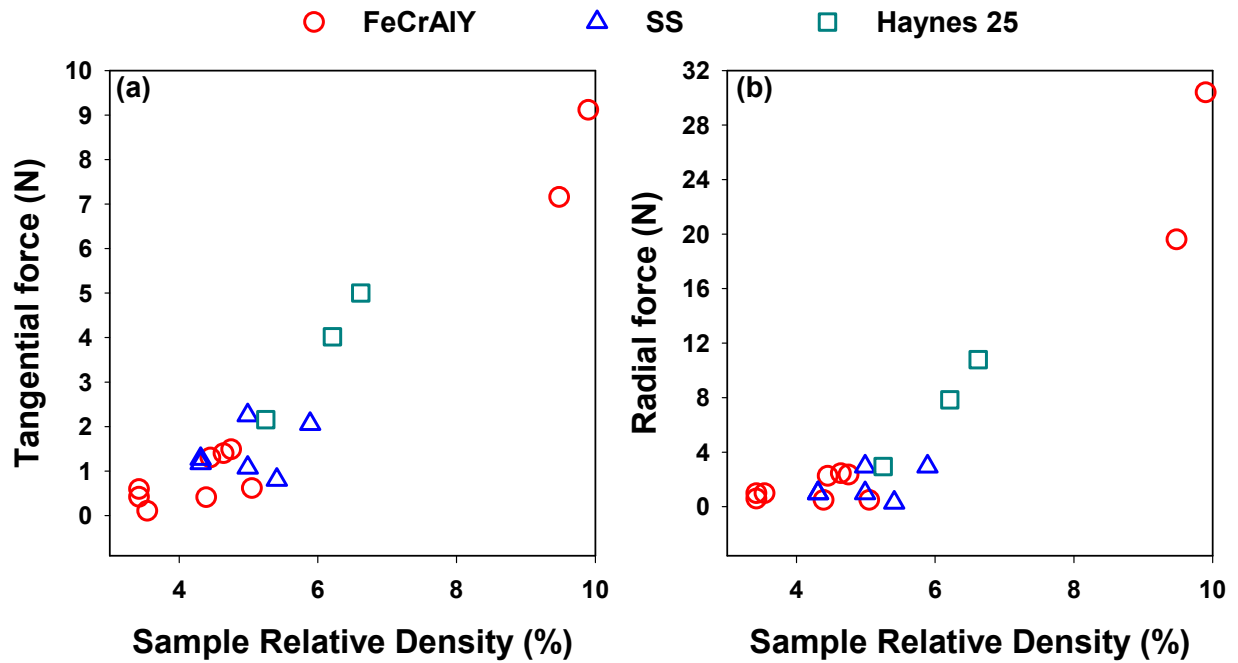


Figure 7.—Rub induced (a) tangential and (b) radial forces as a function of sample relative density.

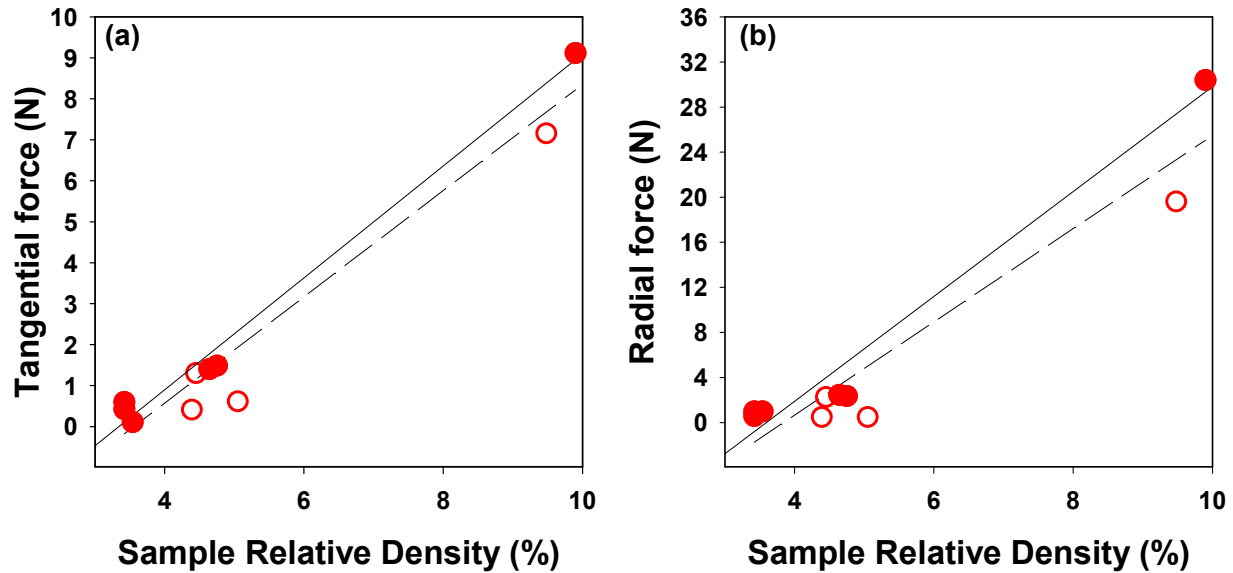


Figure 8.—Rub induced tangential (a) and radial (b) forces as a function of sample relative density for FeCrAlY foams. Trendlines have coefficients of simple determination ( $R^2$  values) of (a) 0.988 for 80 cpi, 0.953 for all samples and (b) 0.967 for 80 cpi, 0.910 for all samples.

## Acoustic Characterization Testing

### Acoustic Characterization Materials

Acoustic test coupons were obtained from a single 25.4 mm (1 in.) thick panel of Haynes 25 foam with nominally 80 cpi and 4.5 percent relative density. The samples were 50.8 by 50.8 mm (2 by 2 in.) with approximate thicknesses of 20 mm (0.8 in.) and 10 mm (0.4 in.). Two thicknesses were used in these tests to allow determination of characteristic impedance and propagation constant via the two thickness techniques described by Smith and Parrott (Ref. 5). Determination of these key material acoustic properties can be used to establish the metal foam's acoustic uniformity. The square faces of the specimens were prepared by five techniques. The as-received surface is the as-cast surface as provided by the manufacturer. Wire electro-discharge machining (EDM), plunge EDM, and band-saw cutting represent three possible machining techniques. Table III describes the face preparation of the thirteen specimens used in the acoustic study.

TABLE III.—IDENTIFICATION, SURFACE CONDITION, AVERAGE THICKNESS, AND RELATIVE DENSITY FOR IMPEDANCE TUBE SAMPLES

ID	Face A	Face B	Thickness, mm	Relative density, percent
H01	Band saw	As-received	20.8	5.6
H02	Band saw	As-received	11.2	4.3
H03	Band saw	As-received	11.3	3.8
H04	Plunge EDM	Wire EDM	20.4	6.2
H05	Plunge EDM	Wire EDM	20.4	6.7
H06	Plunge EDM	Wire EDM	10.2	6.1
H07	Tip rub	Wire EDM	20.2	6.7
H08	Tip rub	Wire EDM	20.7	7.2
H09	Tip rub	Wire EDM	10.1	4.8
H10	Wire EDM	As-received	20.3	4.5
H11	Wire EDM	As-received	20.9	4.5
H12	Wire EDM	Wire EDM	10.1	4.4
H13	Wire EDM	Wire EDM	10.6	6.5

In order to achieve a rubbed surface over the square face, the two-axis load frame was replaced with a square specimen holder that was translated in two axes by PACS controlled stepper motors. Approximately 2 mm of the specimen surface was rubbed away in sequential 10 mm wide passes. Figure 9 compares scanning electron micrographs of as-received, wire EDM, plunge EDM, band-saw cut, and rubbed surfaces. Both the as-received and wire EDM samples had cell walls and ligaments that ended abruptly at the surface. The plunge EDM process resulted in localized melting that gave the appearance of coarsening the surface. The band-saw cut and rubbed surfaces appeared to have some cell walls or ligaments that were folded over.

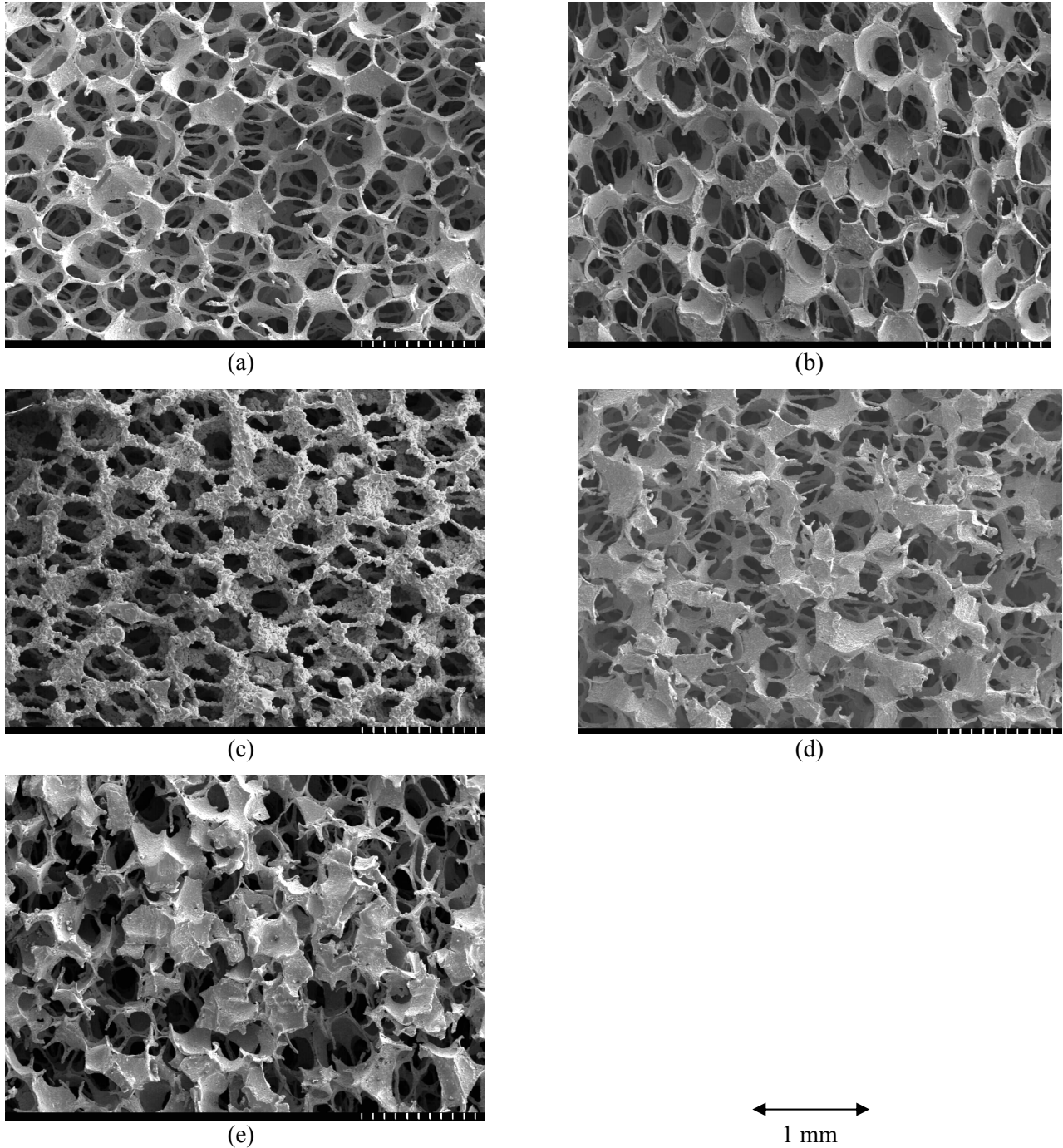


Figure 9.—Haynes 25 metallic foam, 80 cpi, sample surfaces (a) as-received, (b) wire EDM, (c) plunge EDM, (d) band saw, and (e) tip rubbed.

## Acoustic Characterization Experimental Procedures

The frequency-dependent acoustic impedance was determined using the NASA Langley Normal Incidence Tube (Ref. 6). Tests were conducted using a broadband noise source at two overall sound pressure levels (OASPL), 120 and 140 dB. The impedance spectra were calculated using the multipoint method which employs fitting techniques to model acoustic wave propagation based on measured pressure data. Once the standing wave generated by the reflection process is described, the complex reflection factor and related acoustic parameters can be calculated. The impedance spectra then were used to compute the corresponding absorption coefficient spectra using Equation (1):

$$\alpha = \frac{4\theta}{(\theta + 1)^2 + \chi^2} \quad (1)$$

where  $\alpha$  represents the frequency-dependent absorption coefficient and  $\theta$  and  $\chi$  represent the corresponding normalized, frequency-dependent, acoustic resistance and reactance, respectively, as defined in Reference 6. Acoustic resistance and reactance are the real and imaginary components of acoustic impedance and are normalized by the density and sound speed of air, 415 MKS Rayls.

The percent variability, PV, between the sample faces was computed using Equation (2):

$$PV = \sum_{f=1500 \text{ Hz}}^{3000 \text{ Hz}} \left| \frac{\alpha_A(f) - \alpha_B(f)}{\alpha_A(f)} \right| * 100 \quad (2)$$

where  $\alpha_A$  and  $\alpha_B$  represent the absorption coefficients at the  $A$  and  $B$  faces, respectively. The computations are based on the results at and above 1500 Hz, where the results were most consistent since an insufficient number of averages were acquired to achieve smooth results at the lower frequencies.

## Acoustic Characterization Results

Acoustic absorption coefficient comparisons found little variation due to surface preparation. Figure 10 shows the spectra for one of the samples with one tip-rubbed and one wire EDM surface. Graphs comparing the calculated absorption coefficient spectra for all the samples are provided in Appendix B. Comparisons of the educed impedance at the two overall sound pressure levels demonstrated that the impedance of this foam is nearly linear and therefore the acoustic properties are independent of the sound pressure level. This result agrees with previous measurements on similar foam (Ref. 2). Note that the absorption coefficient for these samples was affected by the specimen thickness with the thicker specimens having greater absorption.

A review of the figures provided in Appendix B reveals that the absorption coefficient spectra measured on each face were nearly identical for each specimen, with the exception of sample H08. This sample, with tip-rubbed and wire EDM faces, was the only specimen with faces that yielded notably different absorption coefficient spectra. Moreover, the companion tip-rub specimens (specimen H07 and H09) appeared to have relatively low face-to-face variation.

As a means of quantifying these face-to-face comparisons, Figure 11 provides percent variability between absorption coefficient spectra measured on each face for each of the thirteen (13) test specimens. For all but one sample (H08), the variability is shown to be less than 5 percent between the two faces of each sample. Of particular interest is the comparison of results for the H07 and H08 samples, which were configured to be virtually identical. The H07 sample is shown to have only 2.7 percent variability between the absorption coefficient spectra measured on each face, while the H08 has 7.8 percent variability. The H04 and H05 samples were also configured to be virtually identical, each with plunge EDM and wire EDM faces. The H04 and H05 samples have 1.2 and 2.7 percent variability, respectively. The two specimens with two wire EDM faces (H12 and H13) had 3.7 and 3.2 percent variability between

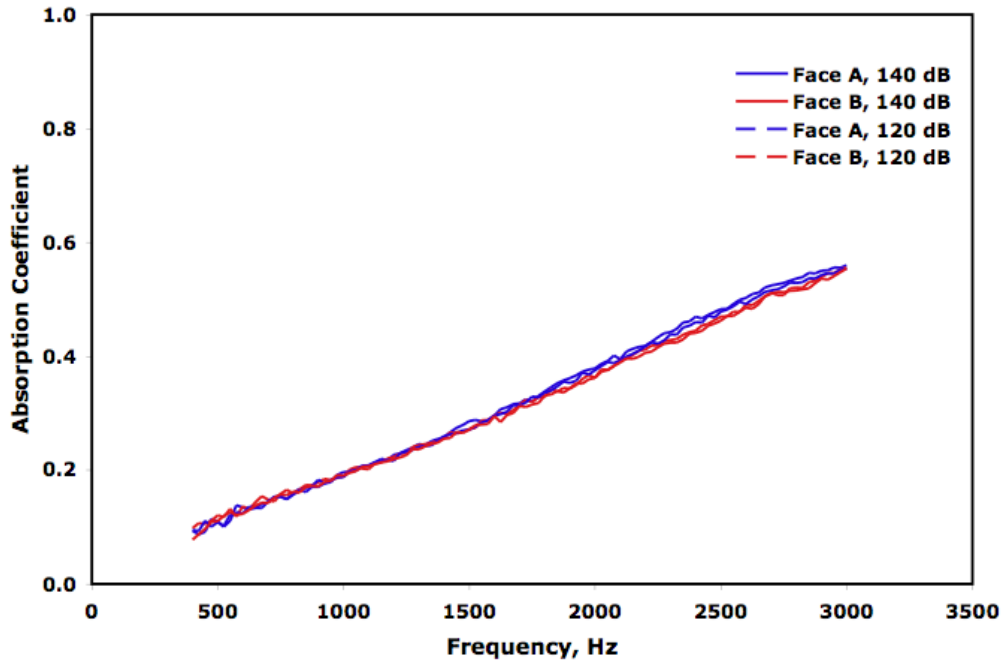


Figure 10.—Absorption coefficient spectra for 20 mm thick specimen H07 comparing tip rub (Face A) and Wire EDM (Face B) faces.

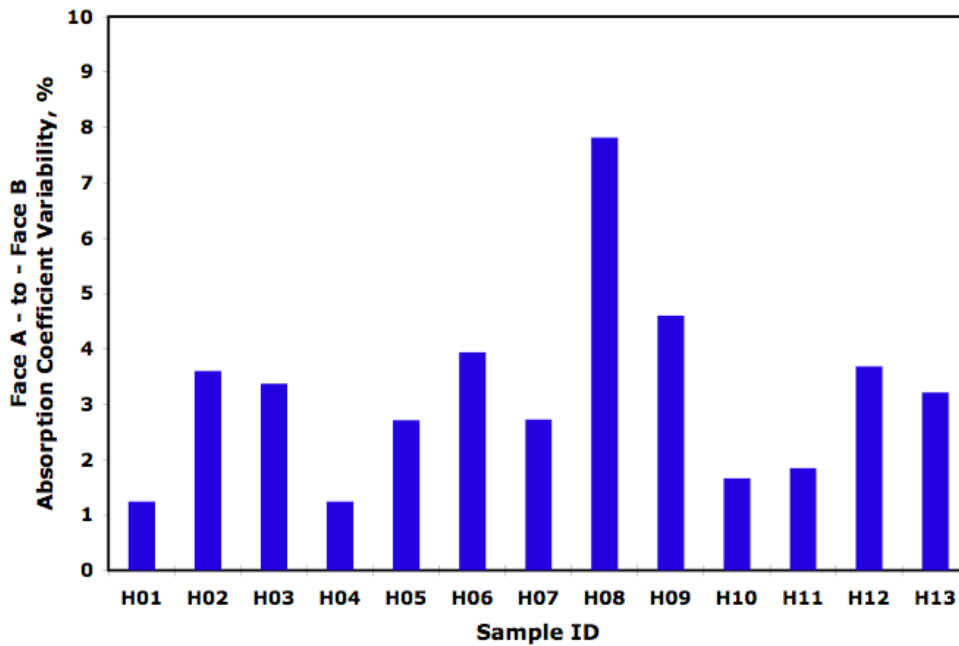


Figure 11.—Face-to-face absorption coefficient spectra variability acquired with 140 dB OASPL broadband noise source.

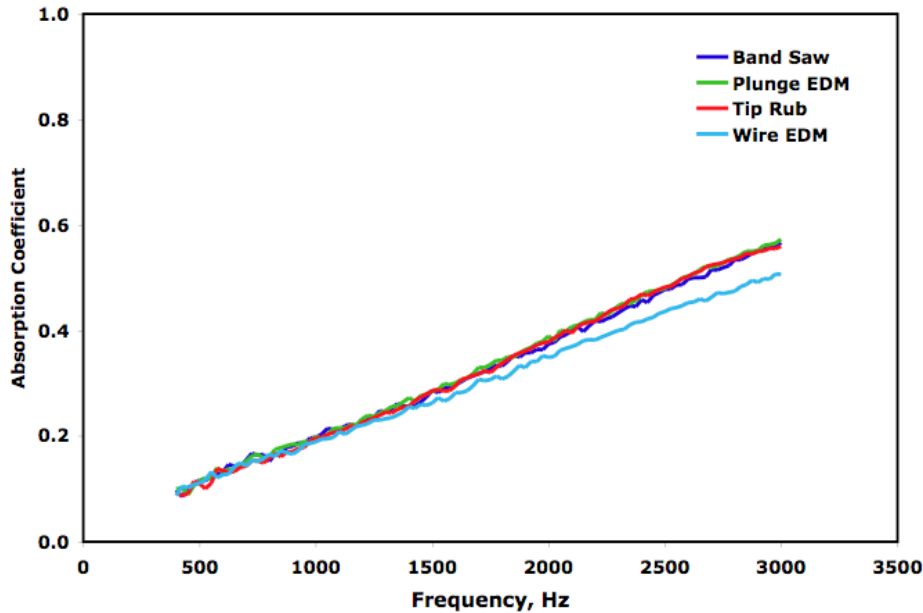


Figure 12.—Absorption coefficient spectra of “A” faces for 20 mm thick specimens with 140 dB OASPL broadband noise source.

their two faces. This inconsistency, in which some of the identical samples give the expected similar levels of variability while others do not, is believed to be at least partially due to the thickness of the samples used in this study. By using relatively thin samples, the absorption coefficient is relatively low. Hence, very small changes can result in noticeable discrepancies in the percent variability estimates. Regardless, these results indicate that acoustic attenuation properties are not greatly dependent on surface preparation. This result is consistent with the surface being only a small fraction of the sample volume interacting with the sound energy.

Comparison of the absorption coefficient spectra also shows that the response was similar for specimens with the same nominal thickness. Figure 12 shows that the absorption response for the “A” Faces of the 20 mm thick specimens. Because the specimens were from the same plate, similar behavior is expected. The 20 mm thick specimens with a wire EDM surface for Face A also happened to have a slightly lower density and that is probably the reason that their absorption response fell slightly lower than the corresponding results for the other three surfaces shown in Figure 12.

## Conclusions

A bench-top test rig was used to simulate the interaction between rotating fan blades and candidate metal foam liner materials. The small magnitude of loading and the minimal surface damage suggest that metal foams could be used over an aircraft engine rotor without a cover sheet. The forces induced by the rubbing were less than 3 N (~0.65 lbf) in both the  $x$  and  $y$  (tangential and radial) directions for foams with nominally 5 percent relative density and up to 30 N (~6.5 lbf) in the radial direction for foams with about 10 percent relative density. Force variations based on alloy type and cell size were not readily apparent and appeared to be secondary effects compared to the relative density.

Visual inspection of the rubbed surfaces revealed no gross change in the cell structure, but the surfaces certainly appeared more rough and dull than the as-received panel faces or surfaces cut by a precise method such as wire electro-discharge machining (EDM). There was no apparent gouging or smearing, even when rubbing over gaps that simulated seams. Microscopy observation of the rubbed surfaces showed some folding of ligaments and cell-wall segments.

One potential way to quantify significant changes in surface morphology is to measure the change in acoustic impedance, which is an intrinsic acoustic property of the metal foam and can be used to compute the absorption coefficient. The frequency-dependent acoustic absorption coefficients of rubbed surfaces were compared to that of as-received, wire EDM, plunge EDM, and band-saw cut surfaces. All samples had nearly the same response except for one of the rubbed surfaces, which was deemed to be an outlier. These results suggest that there is no appreciable change in acoustic behavior for a simulated tip-rub event. Likewise, candidate machining techniques were equally successful based solely on acoustic absorption response.

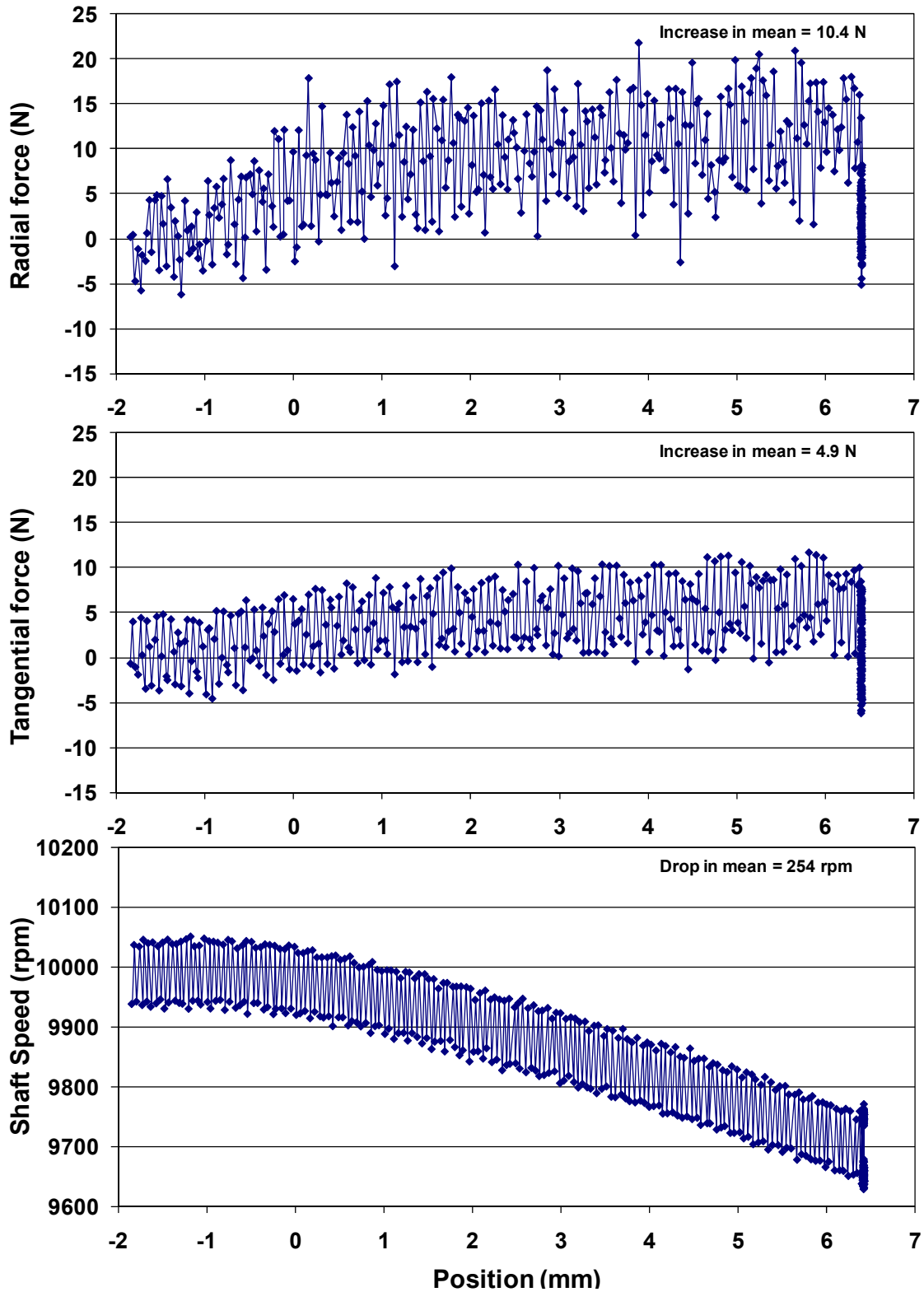
Simulated engine testing has suggested that metal foam acoustic liners offer absorption benefits when positioned directly over the rotating fan blades (Ref. 2). The results presented here indicate that the metallic foams would not be adversely affected by a rub-event. These results suggest that metallic foam acoustic treatments can be considered in future system studies as an over-the-rotor treatment without a protective face sheet.

## References

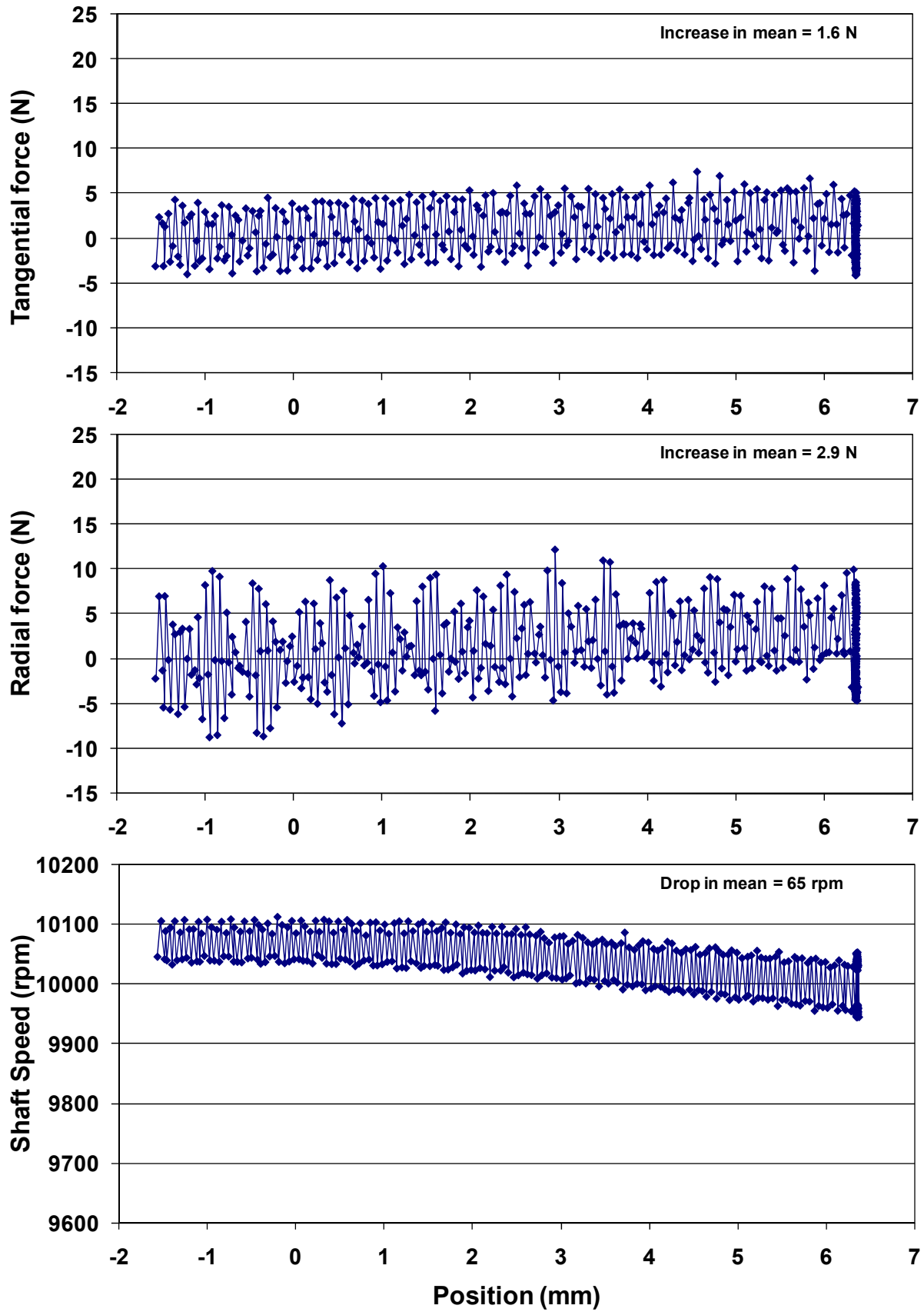
1. Louis-Philippe Lefebvre, John Banhart, and David C. Dunand, "Porous Metals and Metallic Foams: Current Status and Recent Developments," *Advanced Engineering Materials*, 10(9), 2008, pp. 775–787.
2. Daniel L. Sutliff and Michael G. Jones, "Foam-Metal Liner Attenuation of Low-Speed Fan Noise," AIAA–2008–2897, presented at *14th Aeroacoustics Conference* sponsored by American Institute of Aeronautics and Astronautics (AIAA) and Council of European Aerospace Societies (CEAS), Vancouver, British Columbia, Canada, May 5–7, 2008 (also available as NASA/TM—2008-215227 from <http://gltrs.grc.nasa.gov>).
3. Mohan G. Hebsur, unpublished research, NASA Glenn Research Center.
4. Jose C. Gonzalez, "Turbomachinery Rub Strip Impact Tests," presented at AIAA Turbine Test Facility Working Group (TTFWG) Meeting, NASA Glenn Research Center, Cleveland, Ohio, November 3, 1999.
5. Charles D. Smith and Tony L. Parrott, "Comparison of Three Methods for Measuring Acoustic Properties of Bulk Materials," *Journal of the Acoustic Society of America*, 74(5), 1983, pp. 1577–1582.
6. Michael G. Jones and Tony L. Parrott, "Evaluation of a Multi-Point Method for Determining Acoustic Impedance," *Mechanical Systems and Signal Processing*, 3(1), 1989, pp. 15–35.

## Appendix A.—Tip Rub

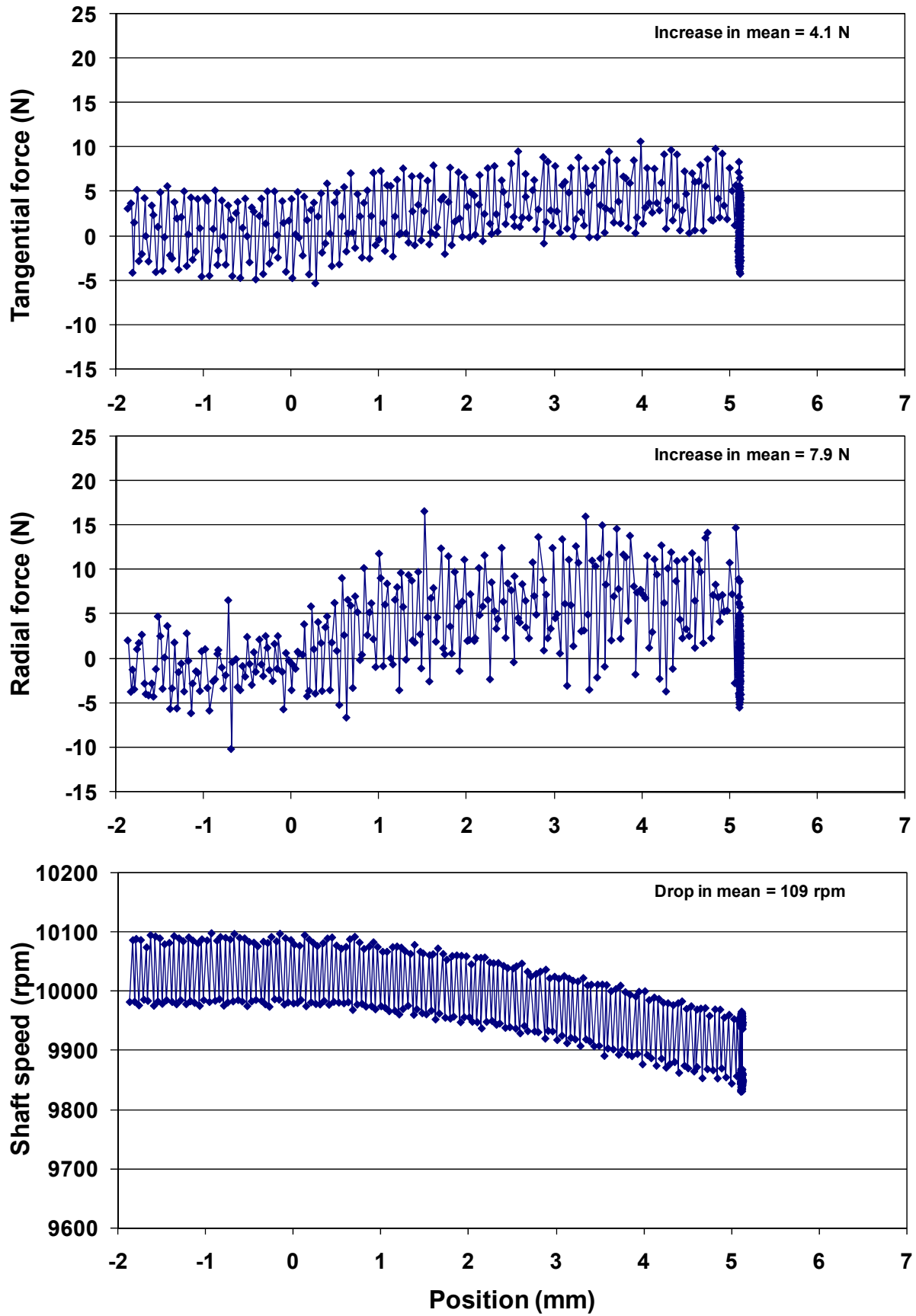
HAY-80-E: 80 cpi, panel  $\rho^* = 4.6$  percent, specimen  $\rho^* = 6.6$  percent, 12.7 mm thick



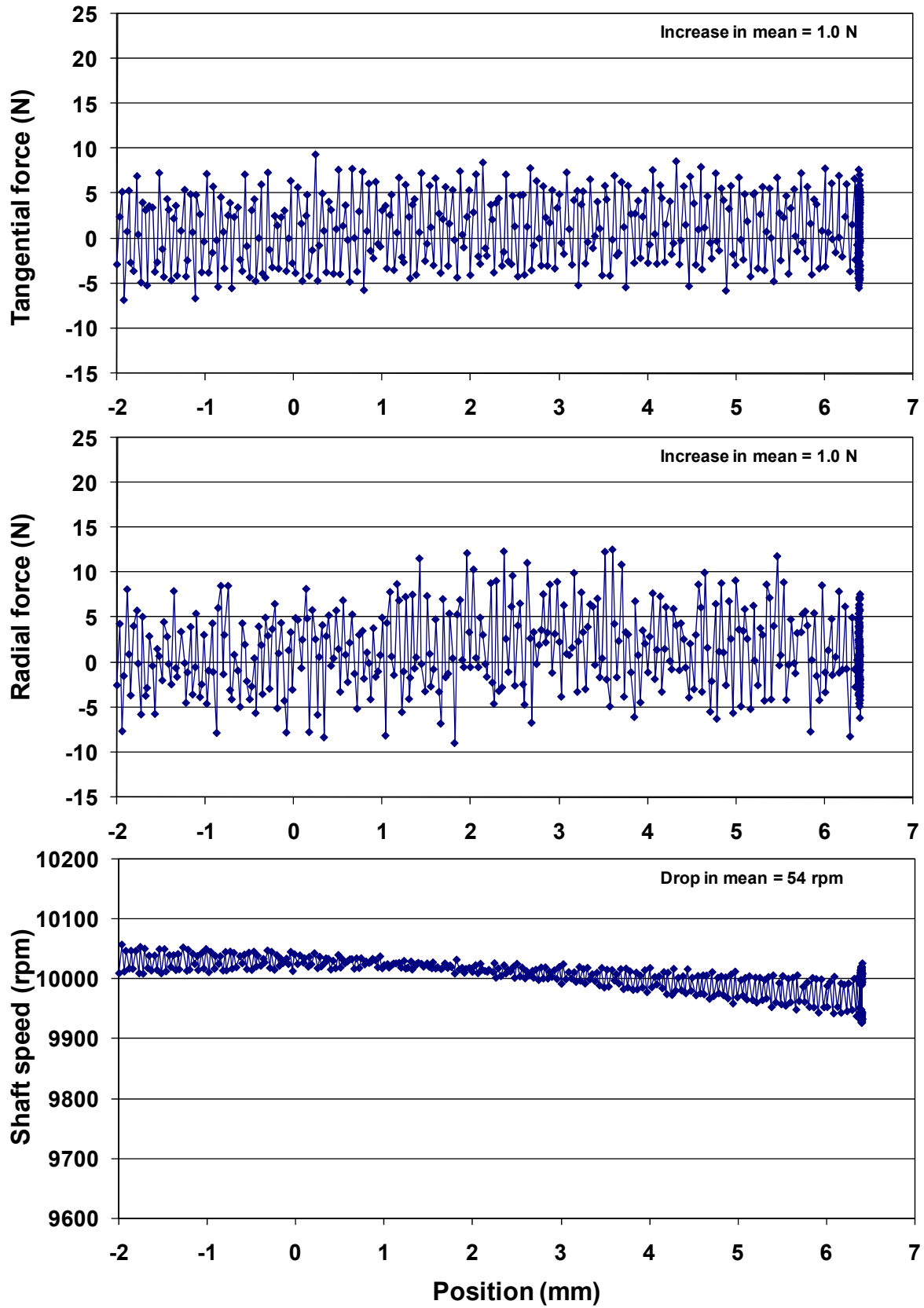
HAY-80-G: 80 cpi, panel  $\rho^* = 6.4$  percent, specimen  $\rho^* = 5.3$  percent, 25.4 mm thick



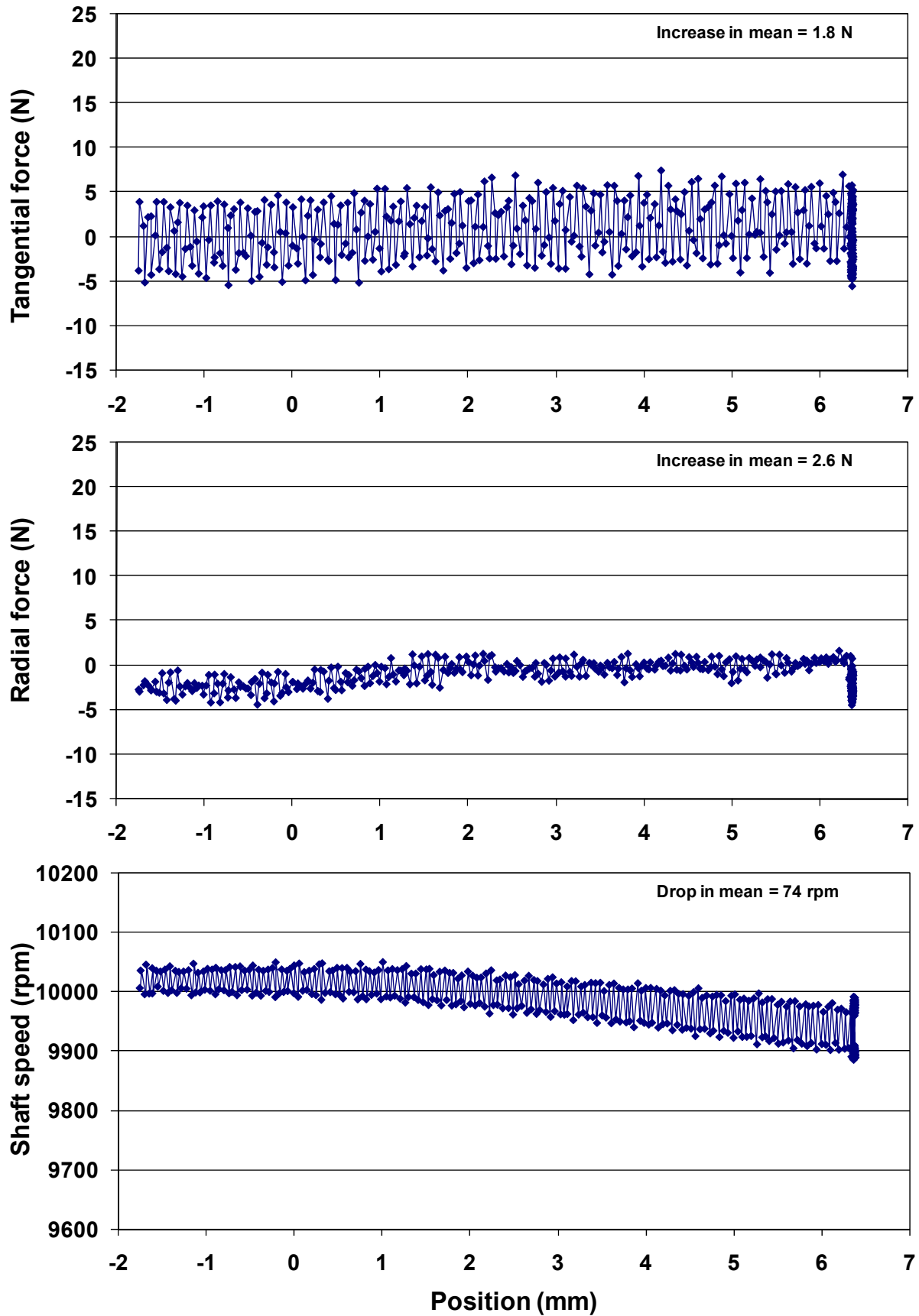
HAY-100-F: 100 cpi, panel  $\rho^* = 6.5$  percent, specimen  $\rho^* = 6.2$  percent, 12.7 mm thick



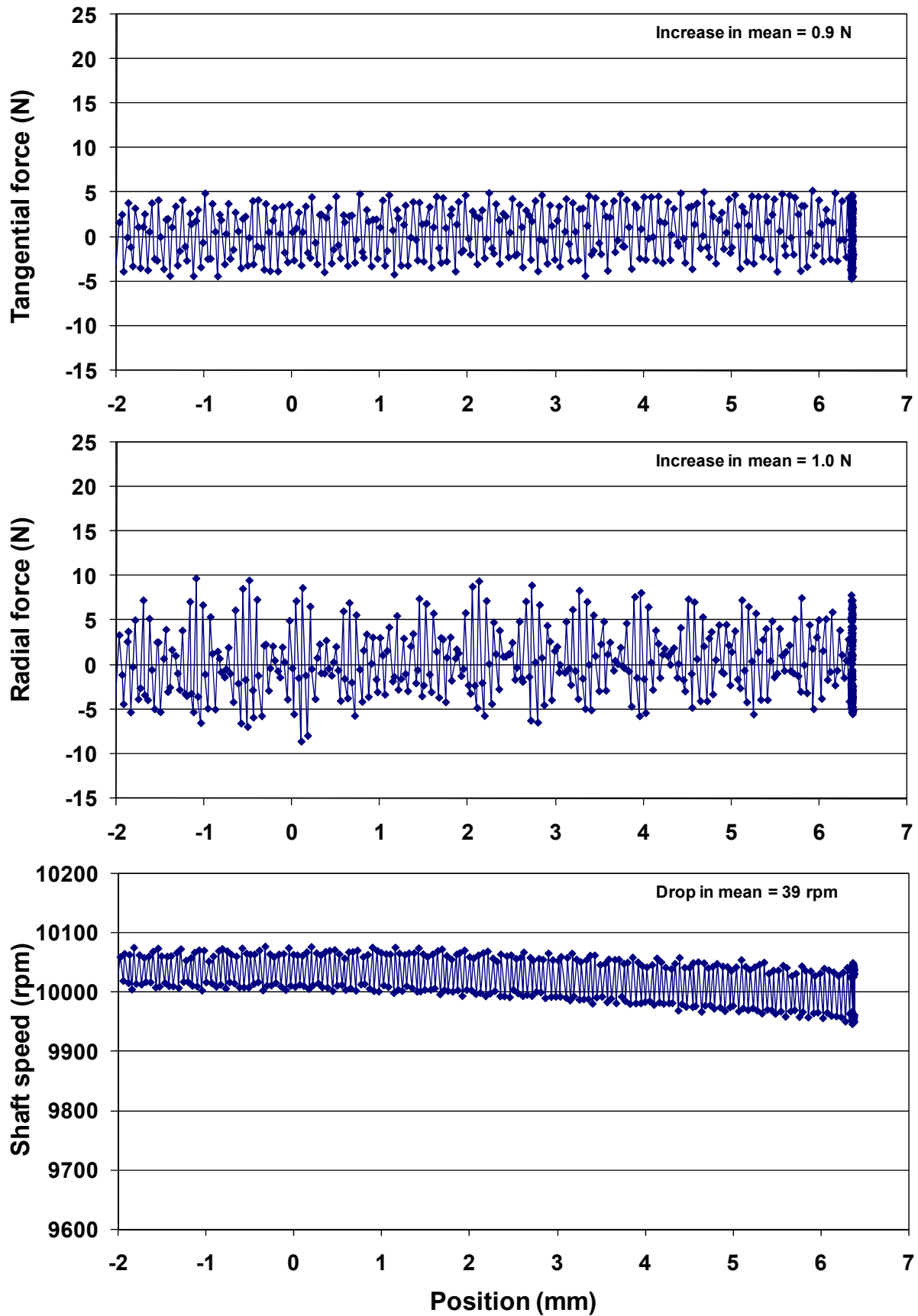
SS316-60-B: 60 cpi, panel  $\rho^* = 5.3$  percent, sample  $\rho^* = 5.0$  percent, 12.7 mm thick



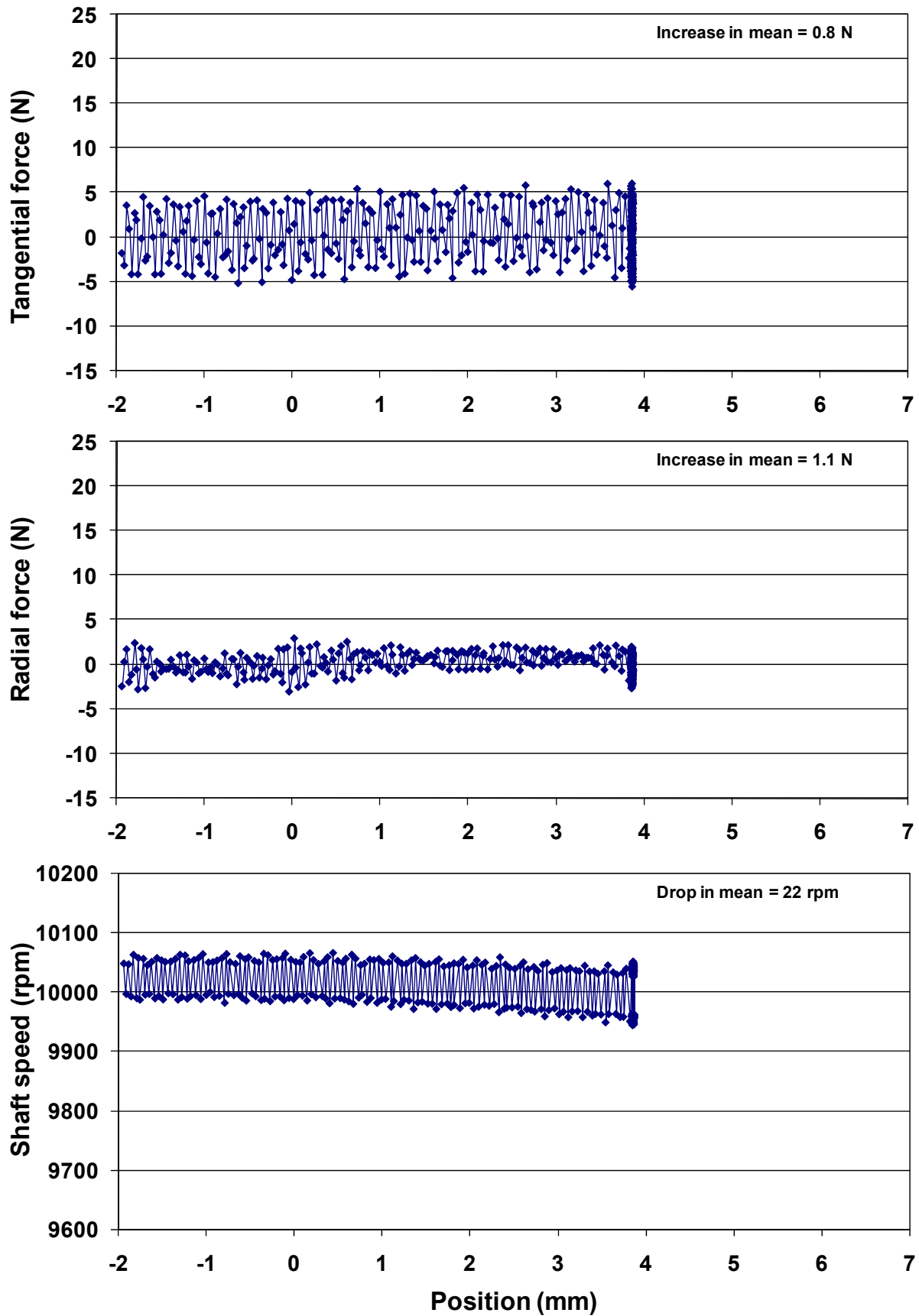
SS316-60-B: 60 cpi, repeat



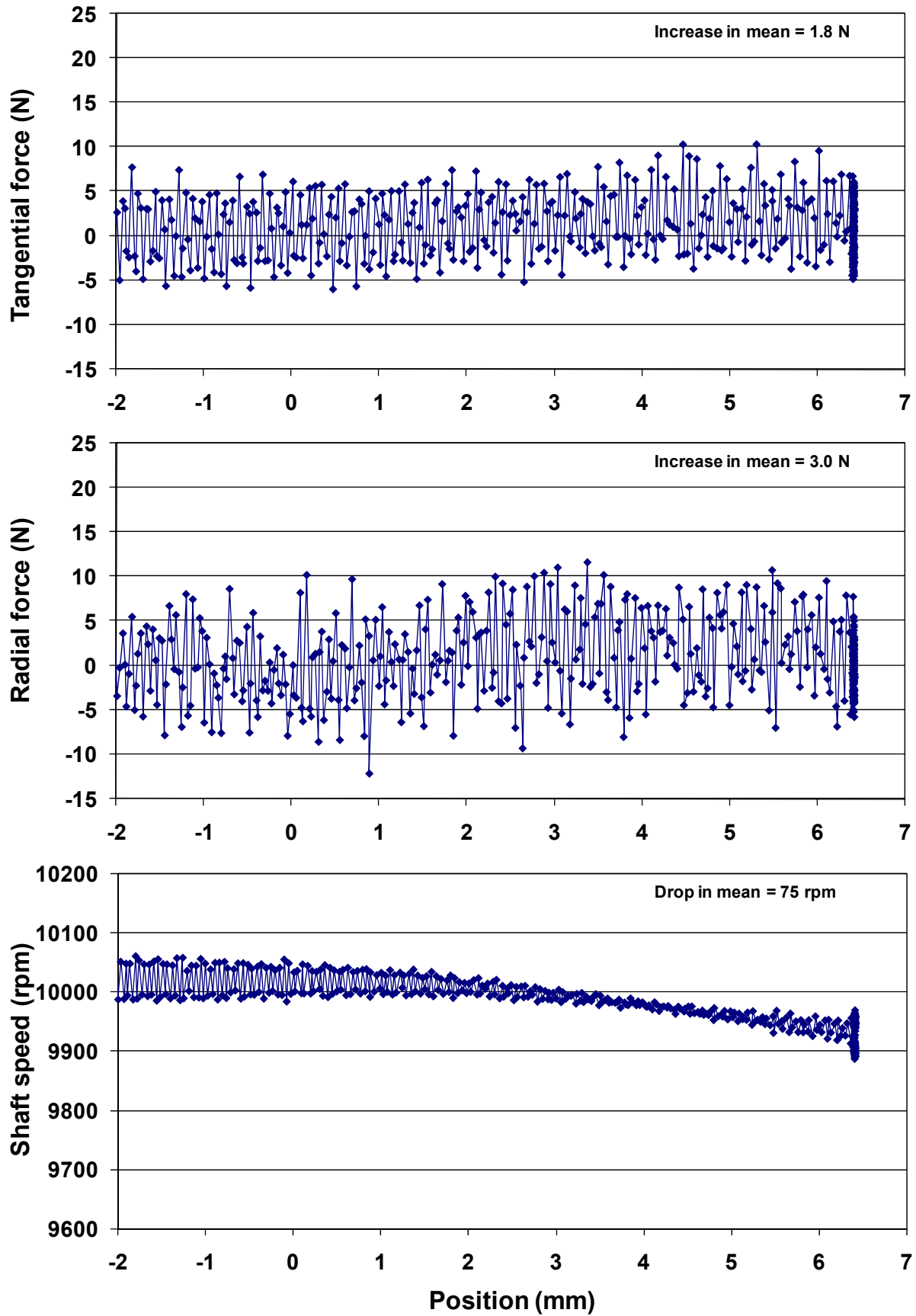
SS314-80-C: 80 cpi, panel  $\rho^* = 4.0$  percent, sample  $\rho^* = 4.3$  percent, 8.9 mm thick



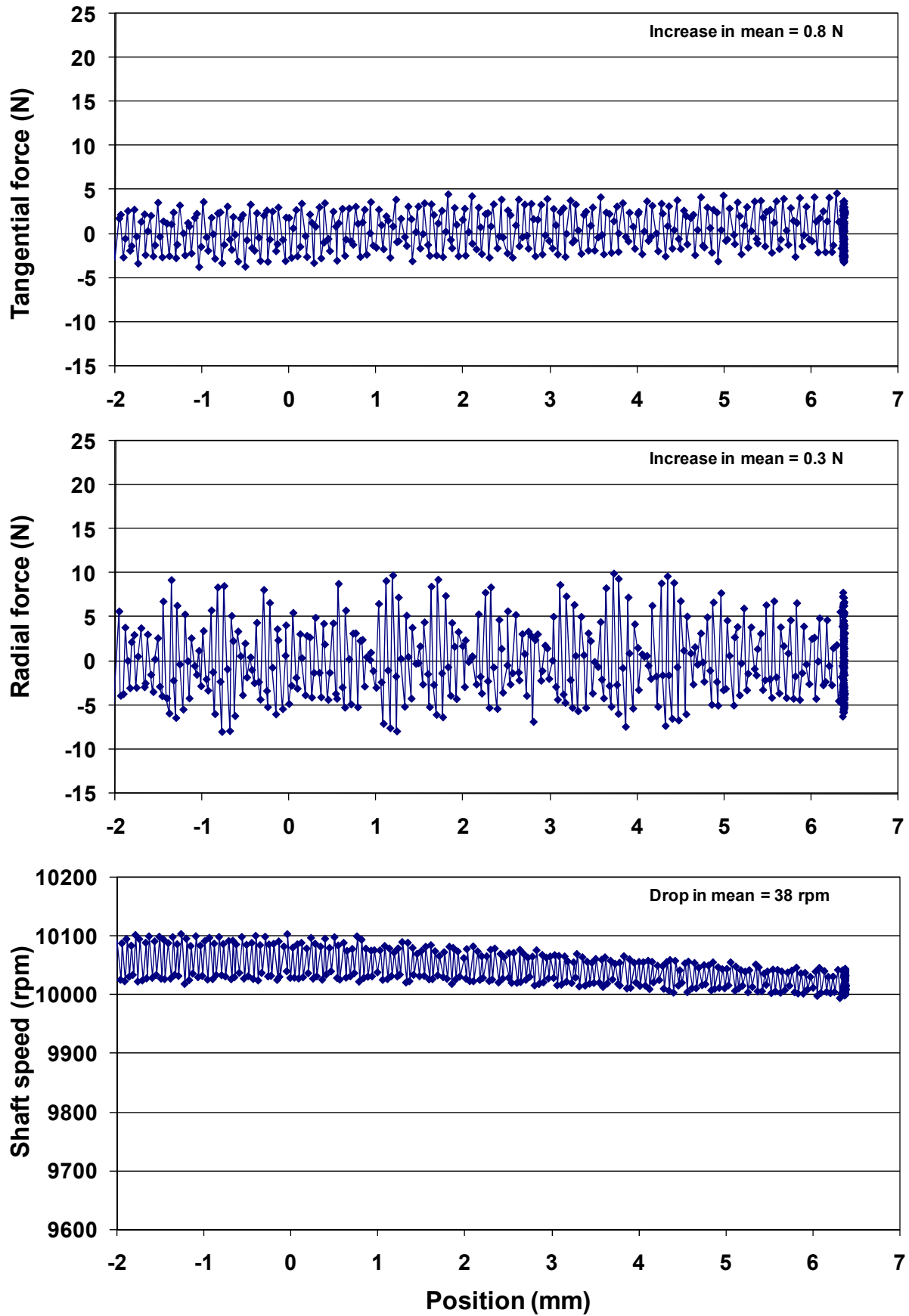
SS314-80-C: 80 cpi, repeat



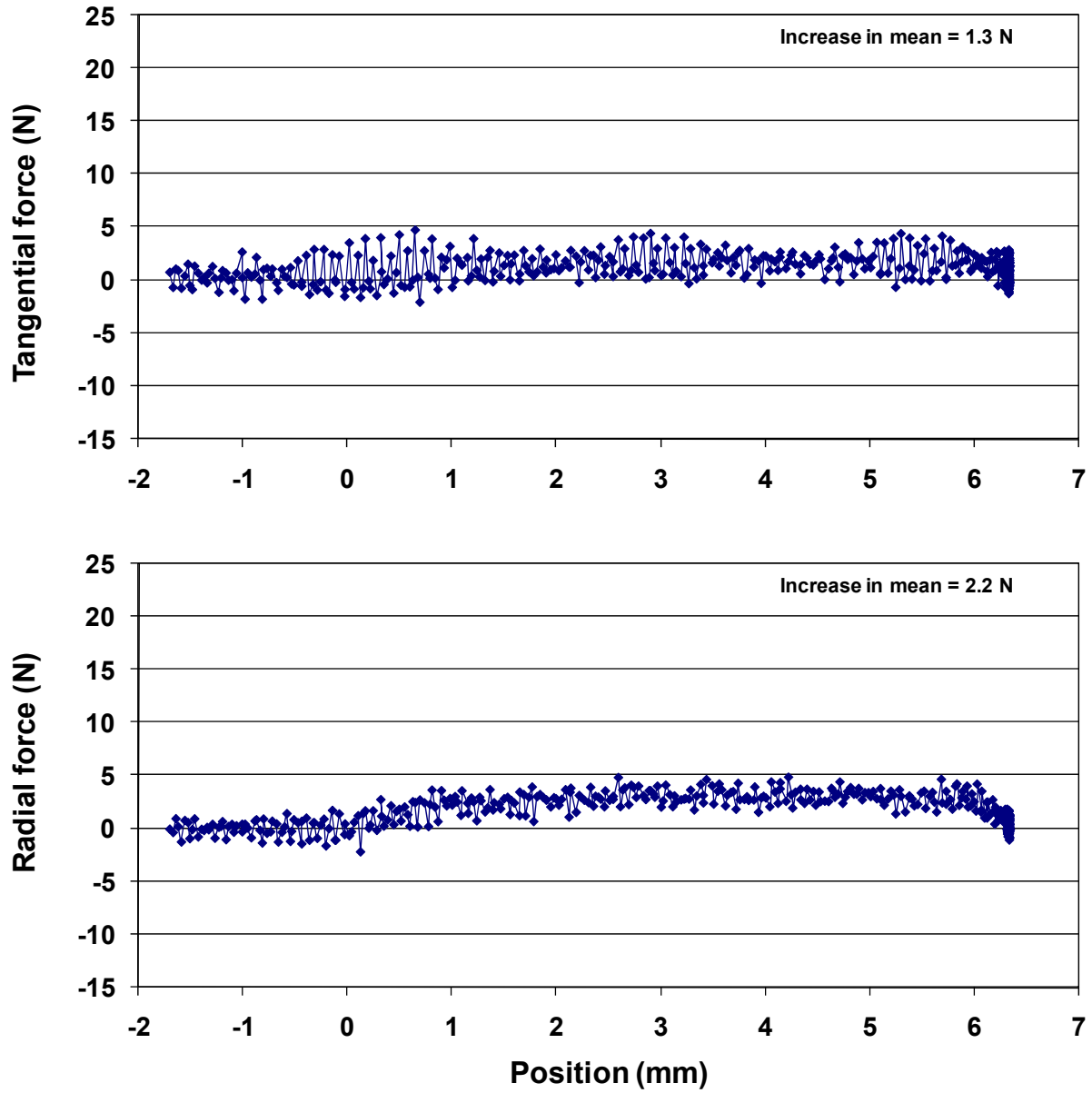
SS316-80-D: 80 cpi, panel  $\rho^* = 5.3$  percent, sample  $\rho^* = 5.9$  percent, 6.4 mm thick



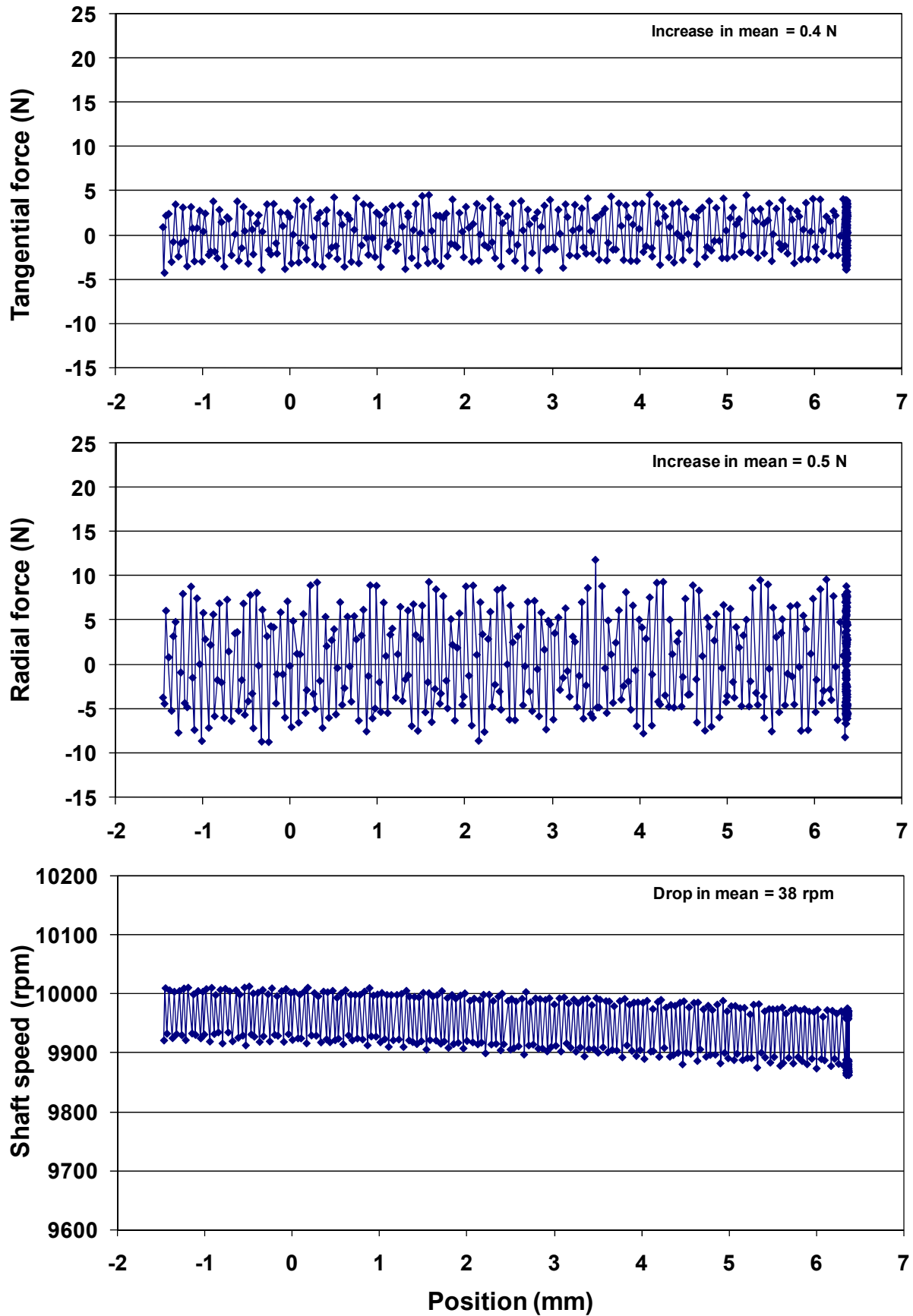
SS316-120-H: 120 cpi, panel  $\rho^* = 5.2$  percent, sample  $\rho^* = 5.4$  percent, 6.1 mm thick



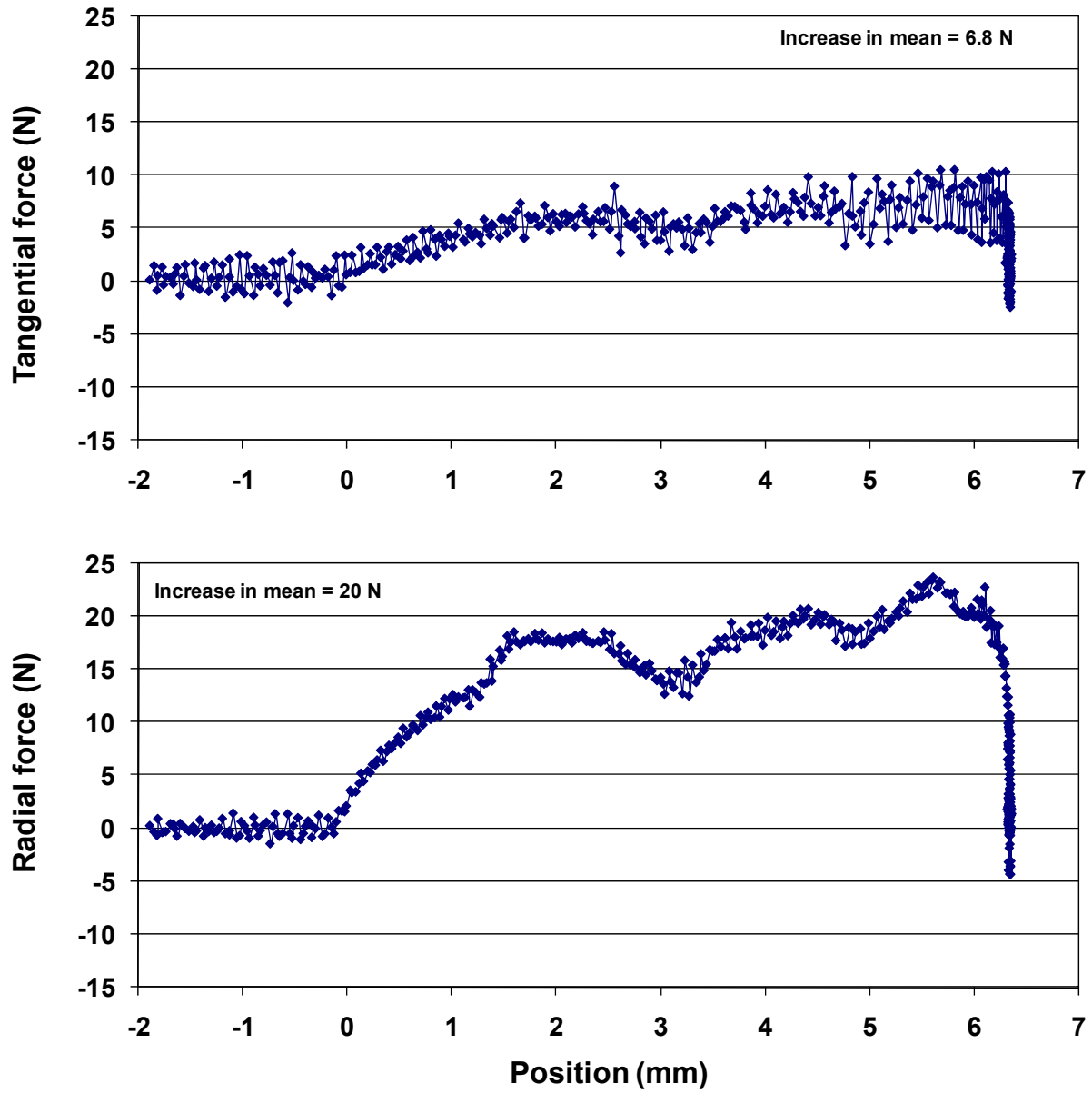
FEC-60-607xviii: 60 cpi, panel  $\rho^* = 4.7$  percent, sample  $\rho^* = 4.5$  percent, 12.5 mm thick  
(shaft speed not recorded)



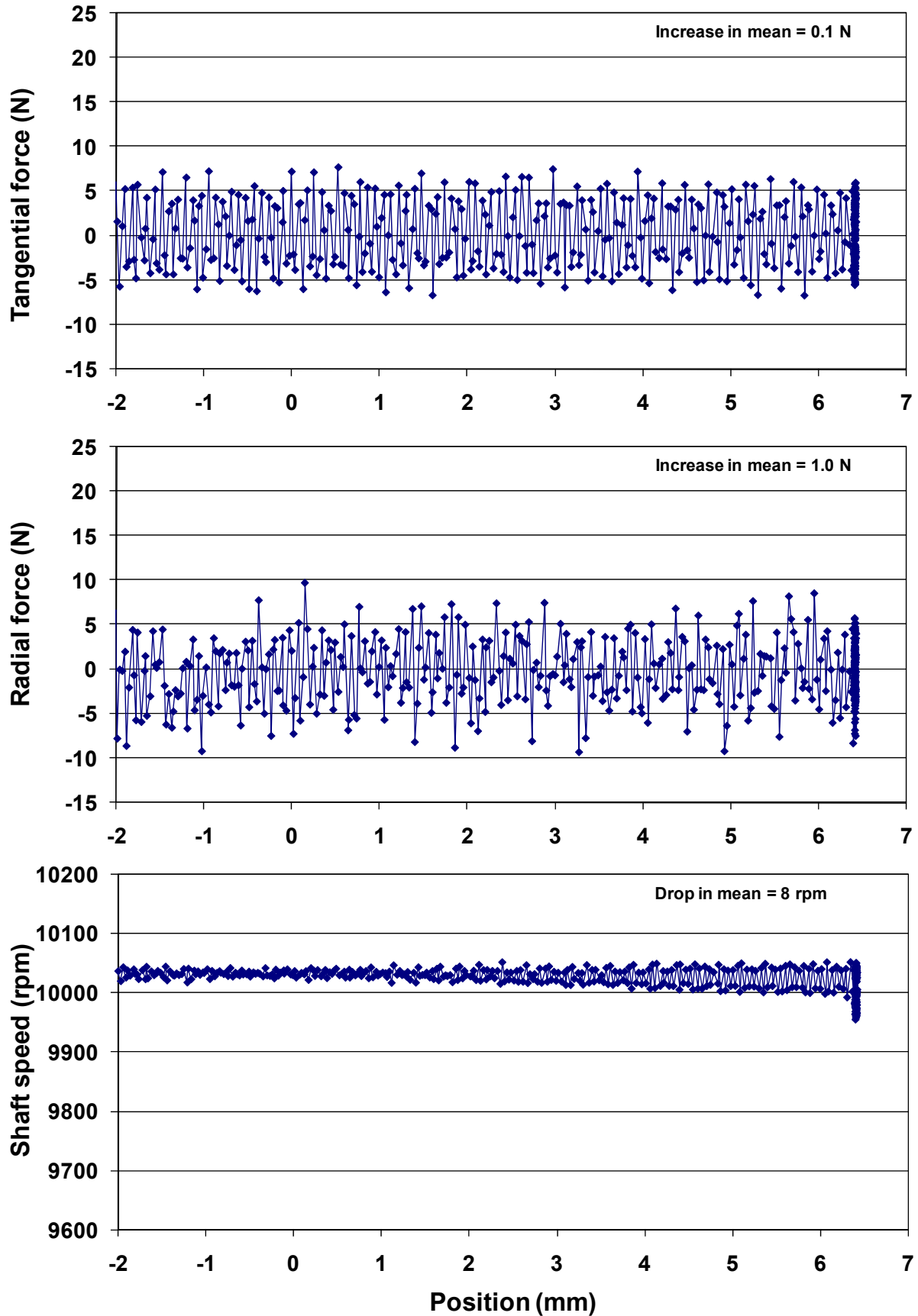
FEC-60-B: 60 cpi, panel  $\rho^* = 5.3$  percent, sample  $\rho^* = 4.4$  percent, 10.2 mm thick



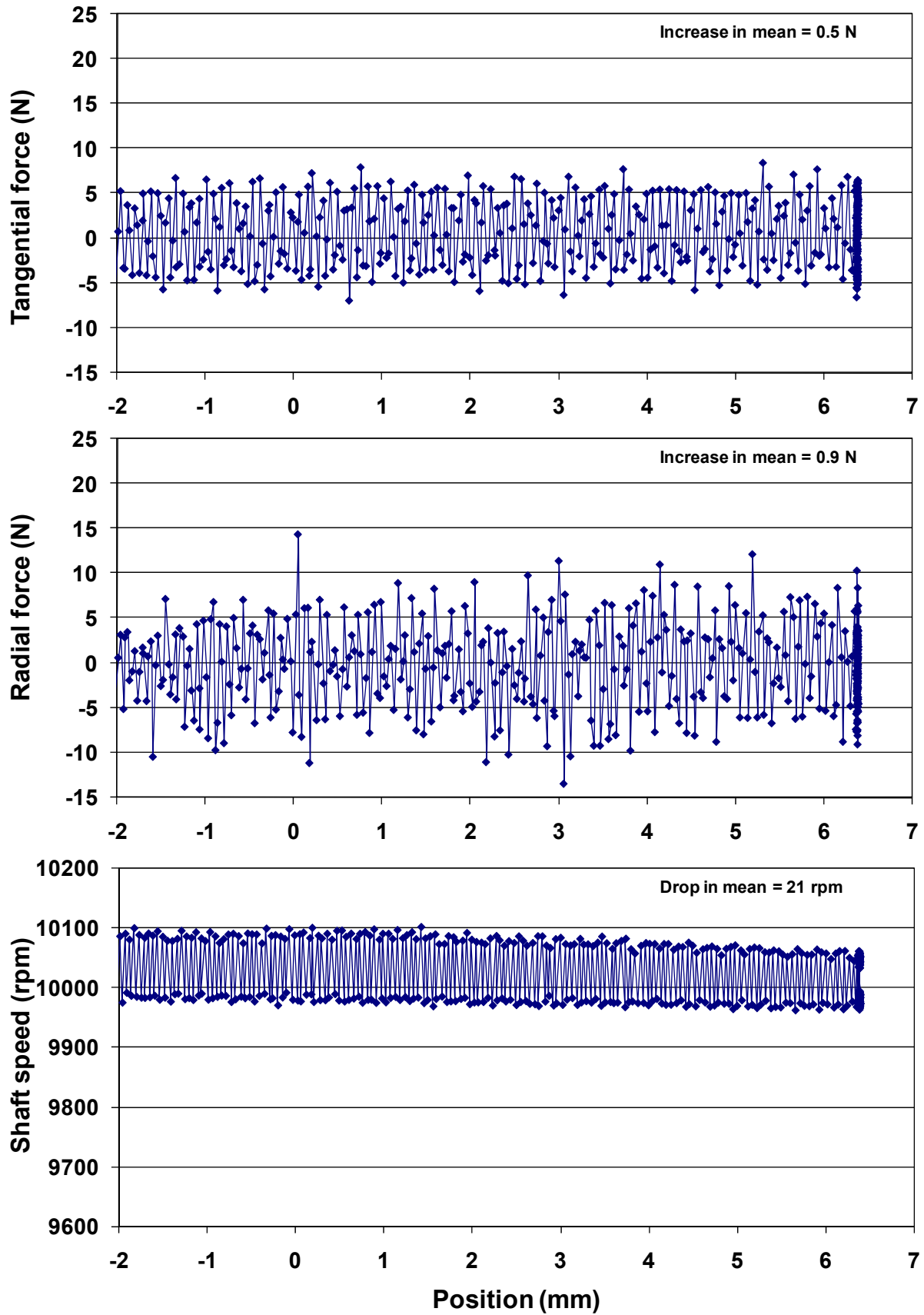
FEC-60-607Axvi: 60 cpi, panel  $\rho^* = 9.7$  percent, sample  $\rho^* = 9.5$  percent, 12.5 mm thick  
(shaft speed not recorded)



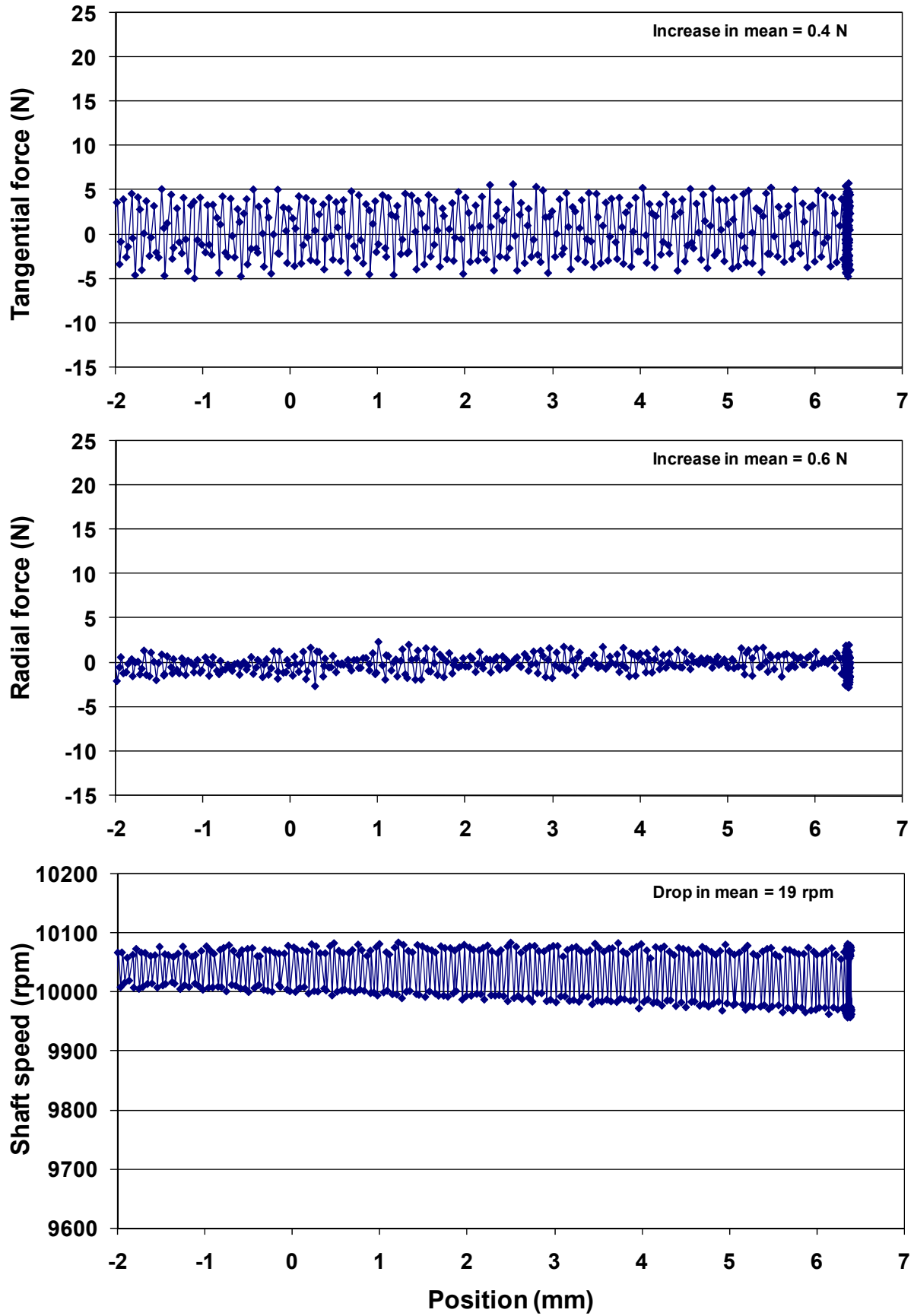
FEC-80-C: 80 cpi, panel  $\rho^* = 2.9$  percent, sample  $\rho^* = 3.5$  percent, 6.6 mm thick



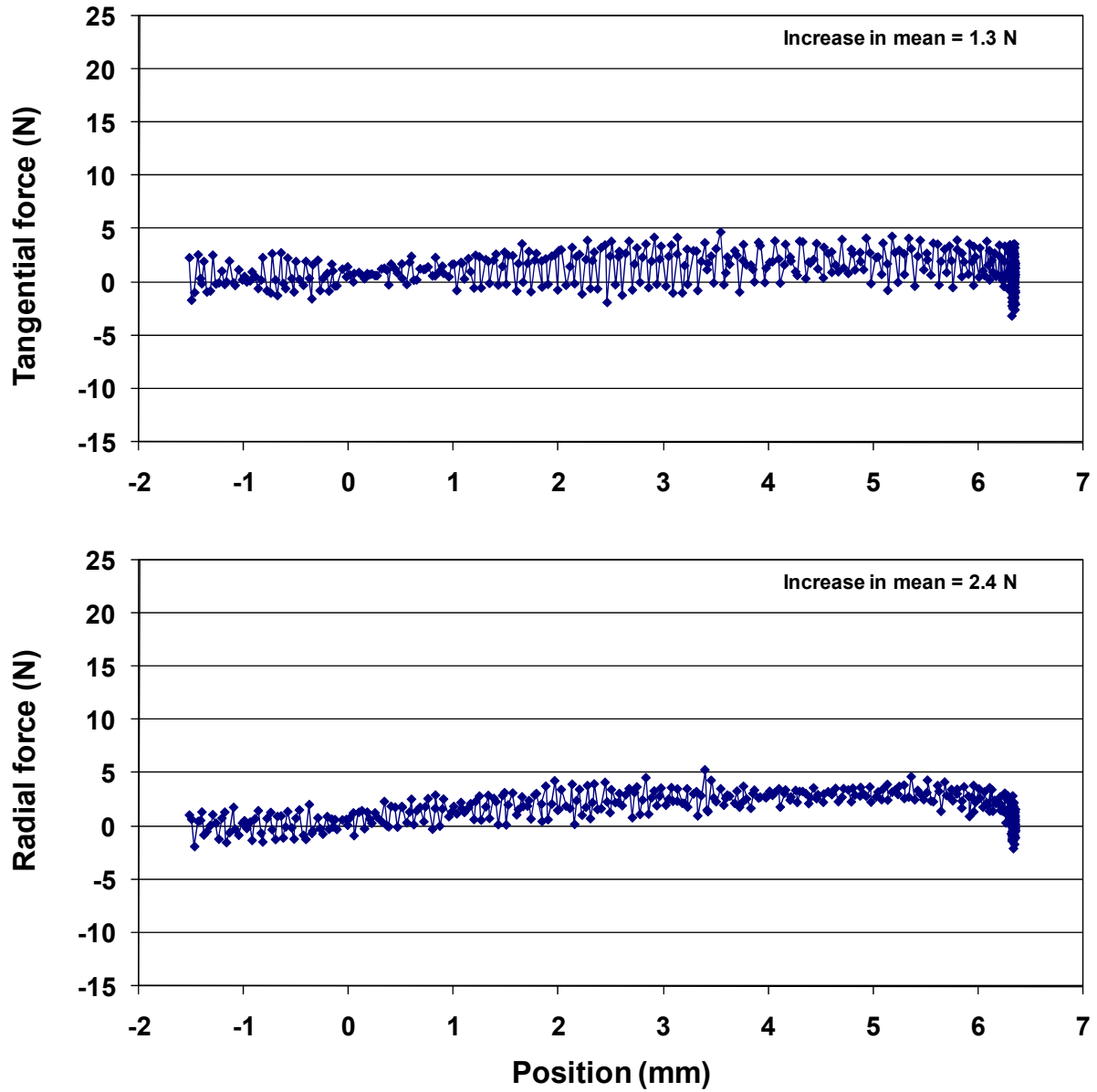
FEC-80-D: 80 cpi, panel  $\rho^* = 4.0$  percent, sample  $\rho^* = 3.4$  percent, 8.9 mm thick



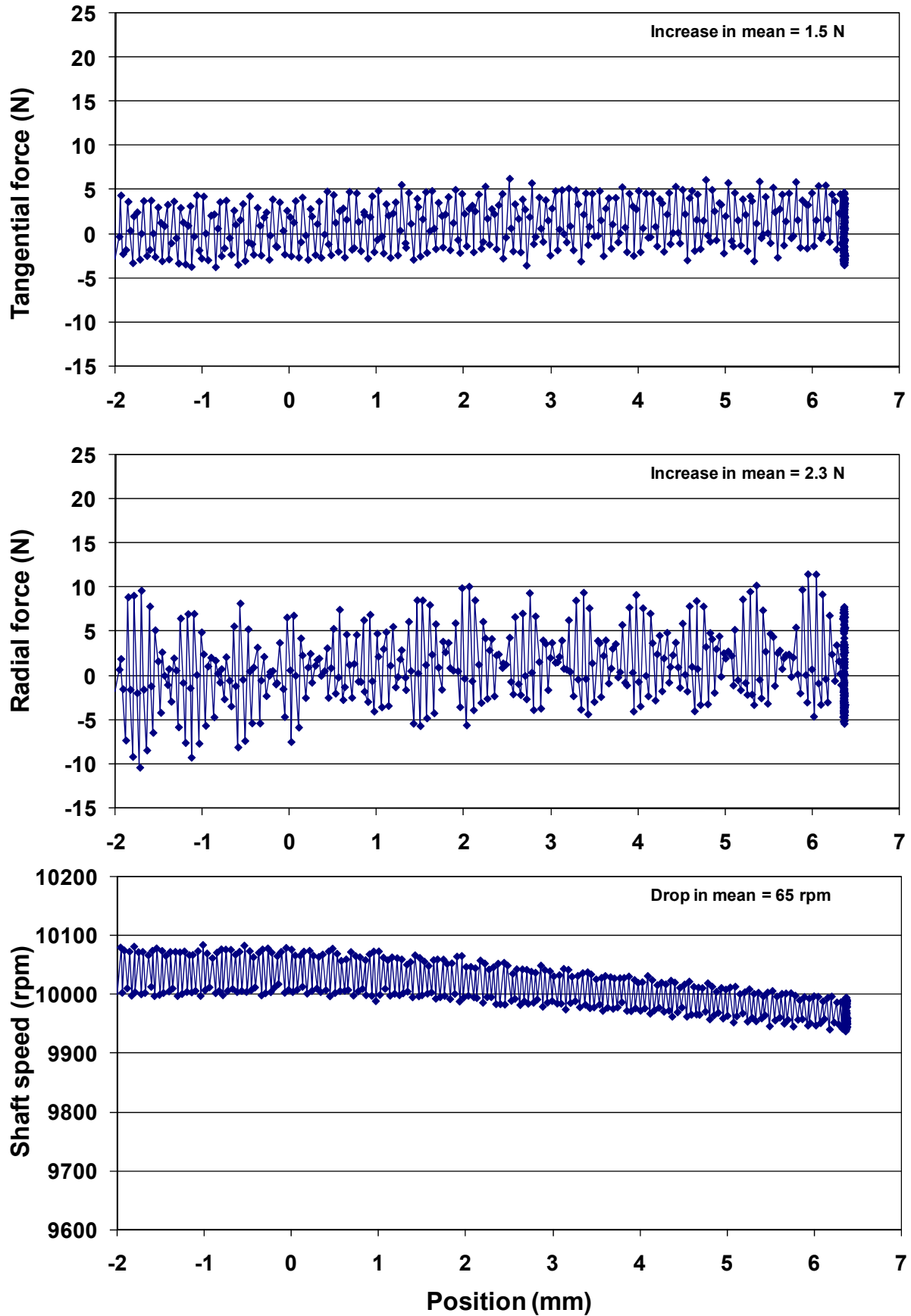
FEC-80-D: 80 cpi, repeat



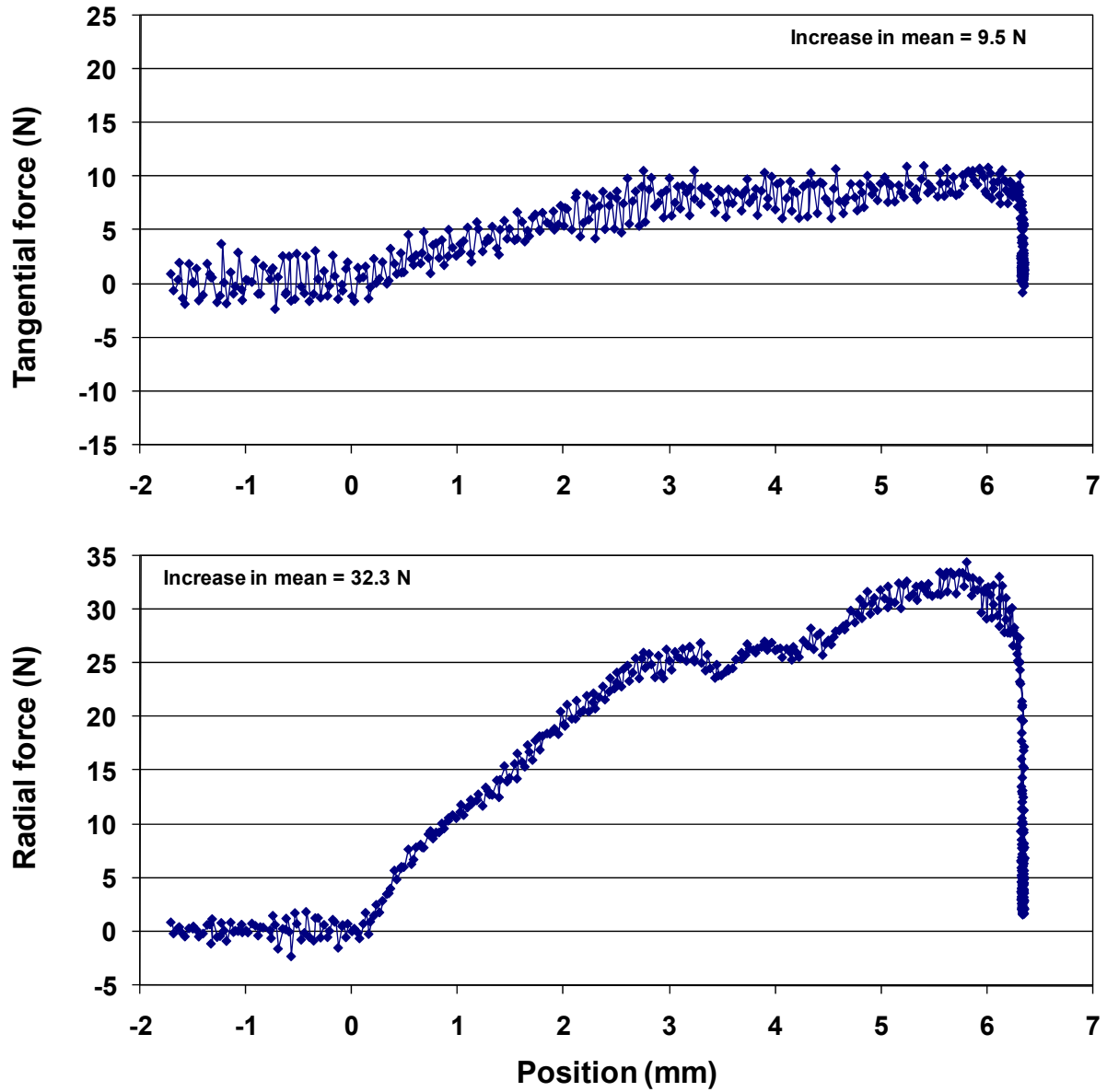
FEC-80-607Bxv: 80 cpi, panel  $\rho^* = 4.8$  percent, sample  $\rho^* = 4.6$  percent, 12.5 mm thick  
(shaft speed not recorded)



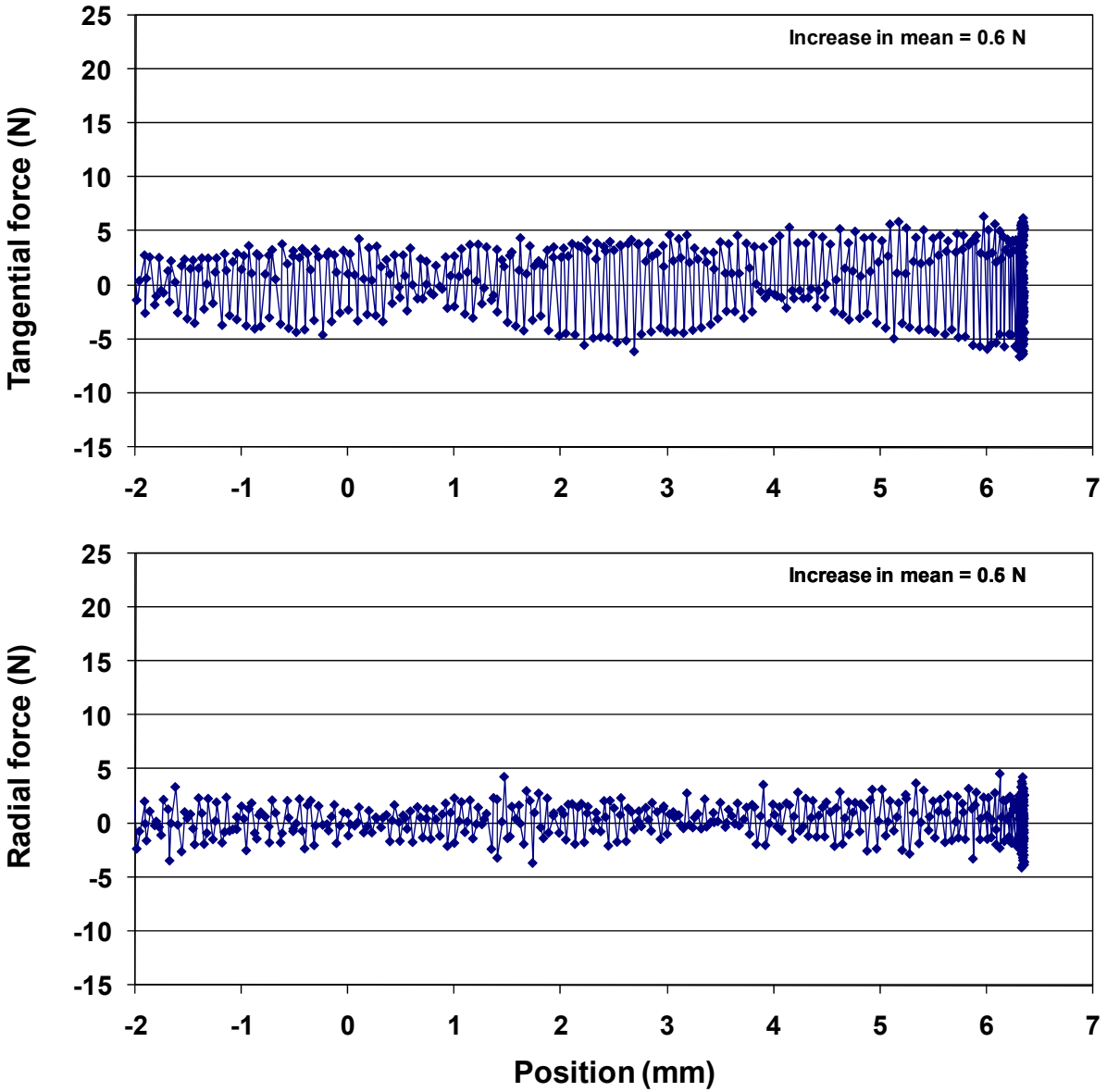
FEC-80-E: 80 cpi, panel  $\rho^* = 5.5$  percent, sample  $\rho^* = 4.8$  percent, 25.4 mm thick



Fe-80-607Di: 80 cpi, panel  $\rho^* = 10.0$  percent, sample  $\rho^* = 9.9$  percent, 12.5 mm thick  
(shaft speed not recorded)



Fe-120-807Div: 120 cpi, panel  $\rho^* = 4.7$  percent, sample  $\rho^* = 5.1$  percent, 12.5 mm thick  
(shaft speed not recorded)

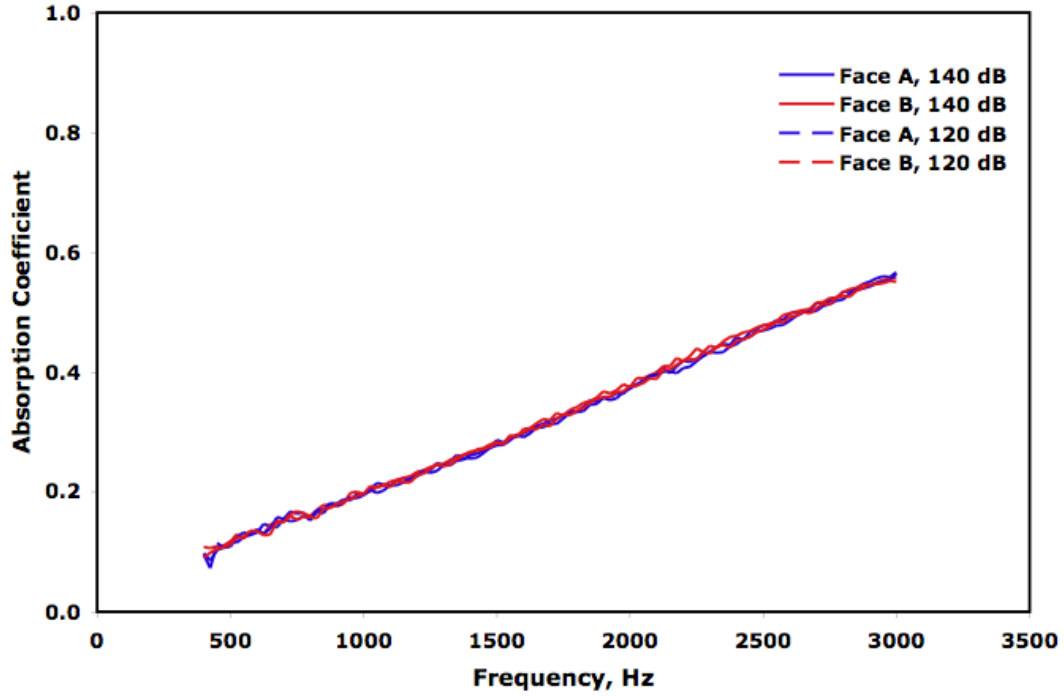




## Appendix B.—Tip Rub

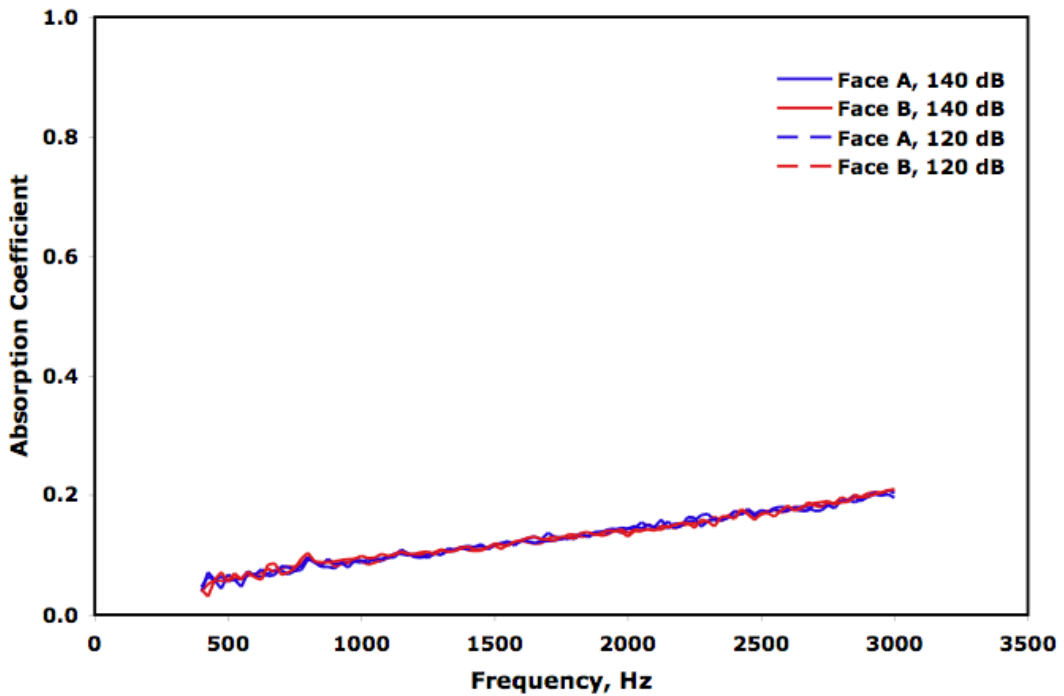
Sample H01

<u>ID</u>	<u>Face A</u>	<u>Face B</u>	<u>Thickness</u>
H01	Band Saw	As-Received	20.8



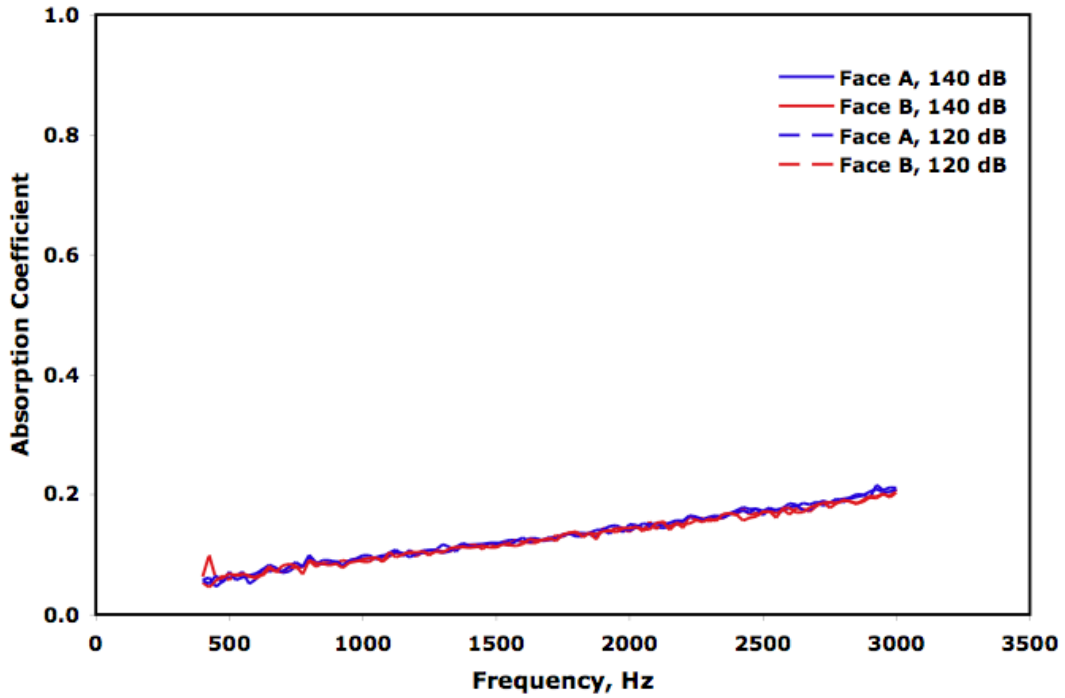
Sample H02

<u>ID</u>	<u>Face A</u>	<u>Face B</u>	<u>Thickness</u>
H02	Band Saw	As-Received	11.2



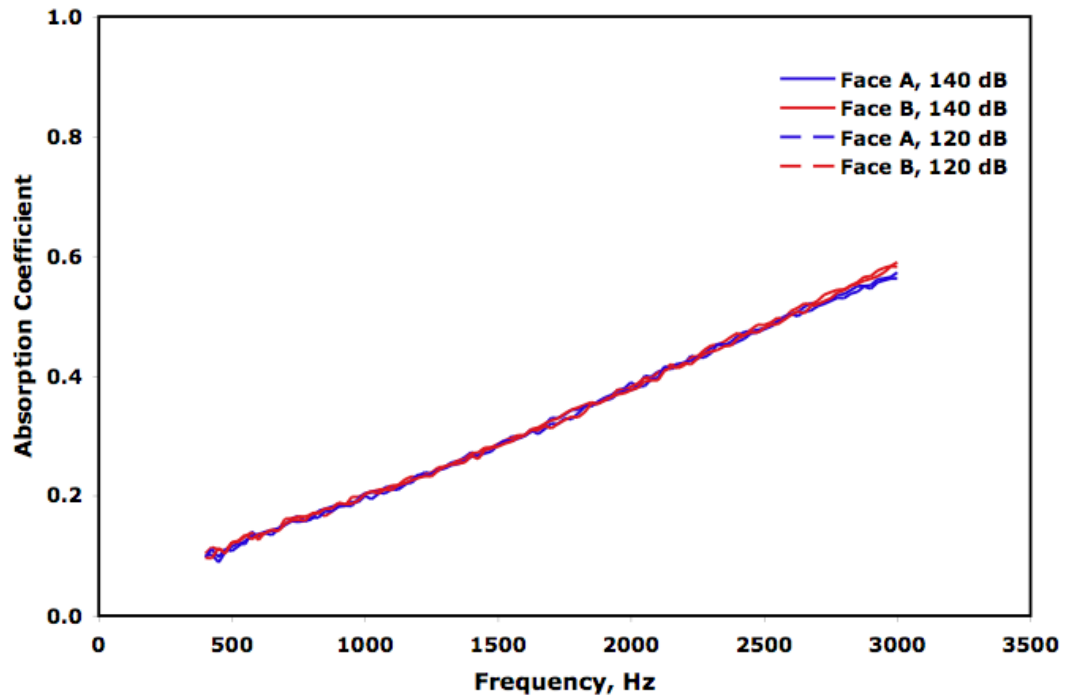
Sample H03

<u>ID</u>	<u>Face A</u>	<u>Face B</u>	<u>Thickness</u>
H03	Band Saw	As-Received	11.3



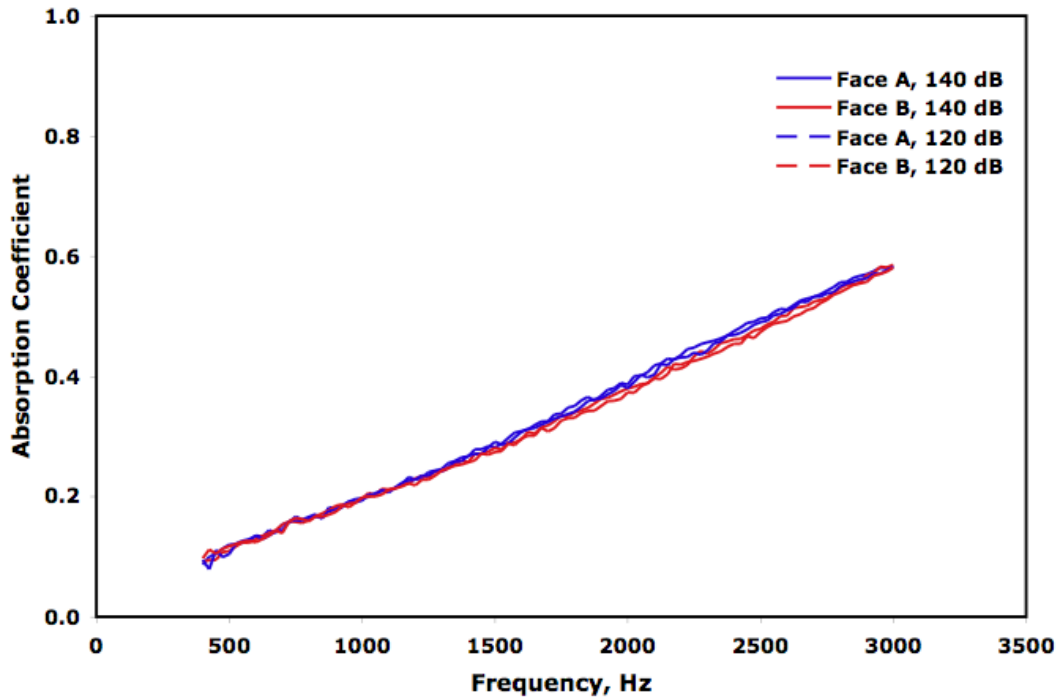
Sample H04

<u>ID</u>	<u>Face A</u>	<u>Face B</u>	<u>Thickness</u>
H04	Plunge EDM	Wire EDM	20.4



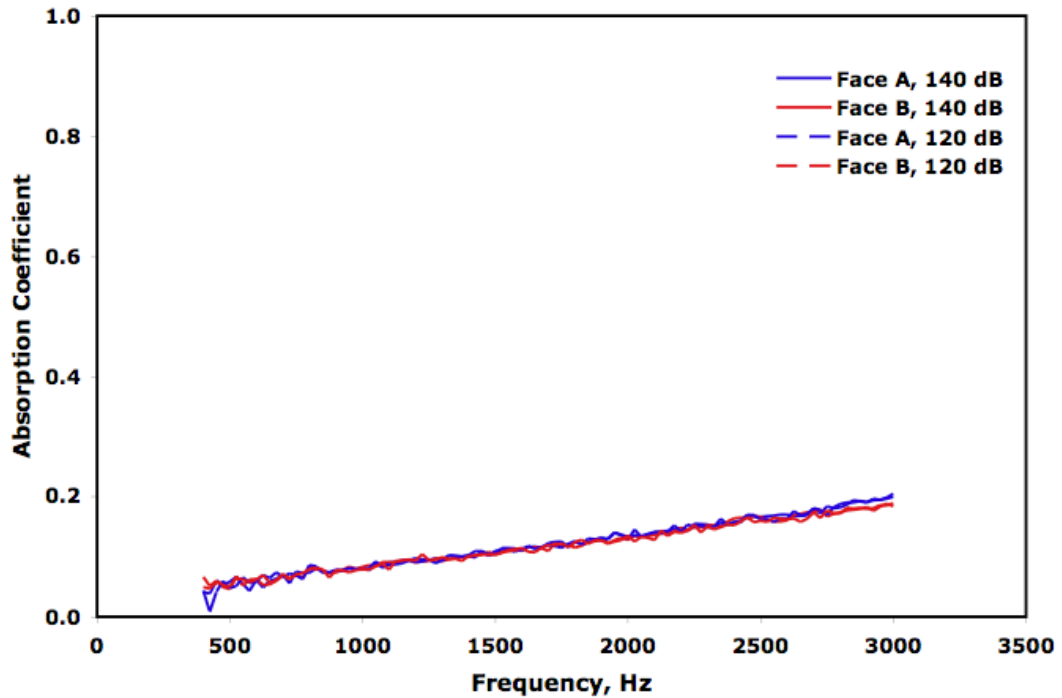
Sample H05

<u>ID</u>	<u>Face A</u>	<u>Face B</u>	<u>Thickness</u>
H05	Plunge EDM	Wire EDM	20.4



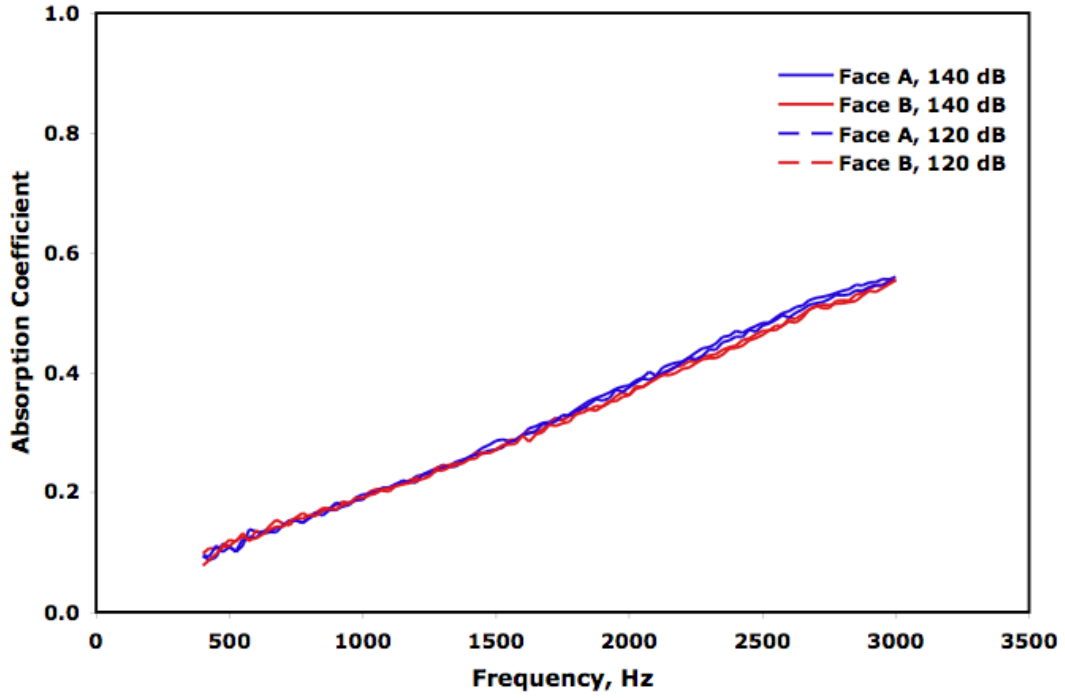
Sample H06

<u>ID</u>	<u>Face A</u>	<u>Face B</u>	<u>Thickness</u>
H06	Plunge EDM	Wire EDM	10.2



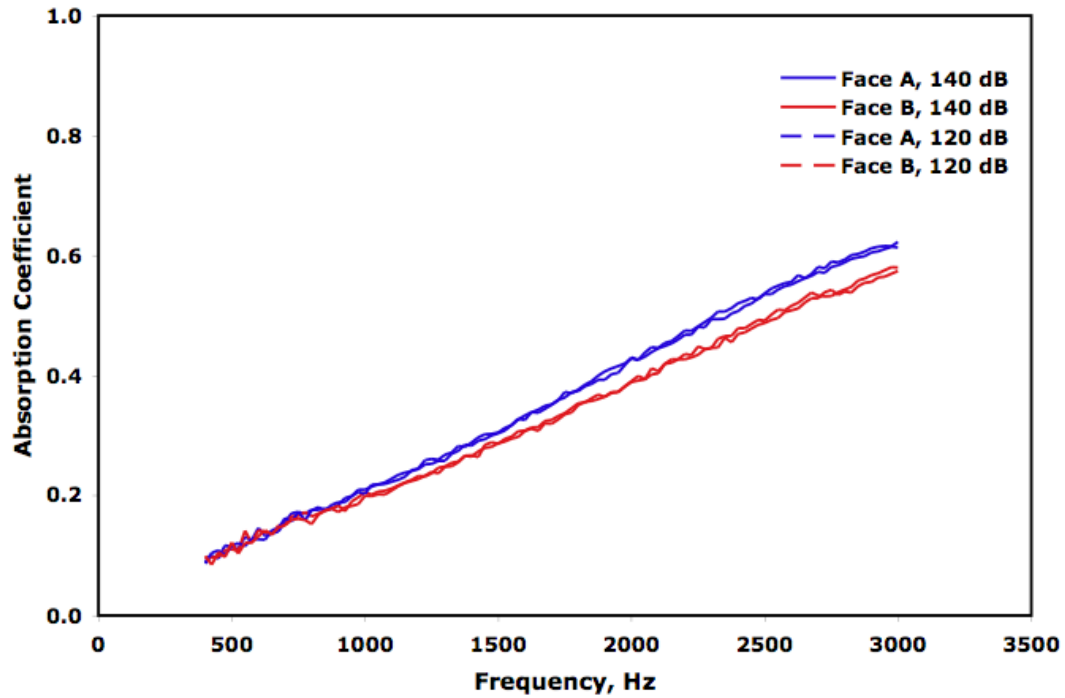
Sample H07

<u>ID</u>	<u>Face A</u>	<u>Face B</u>	<u>Thickness</u>
H07	Tip Rub	Wire EDM	20.2



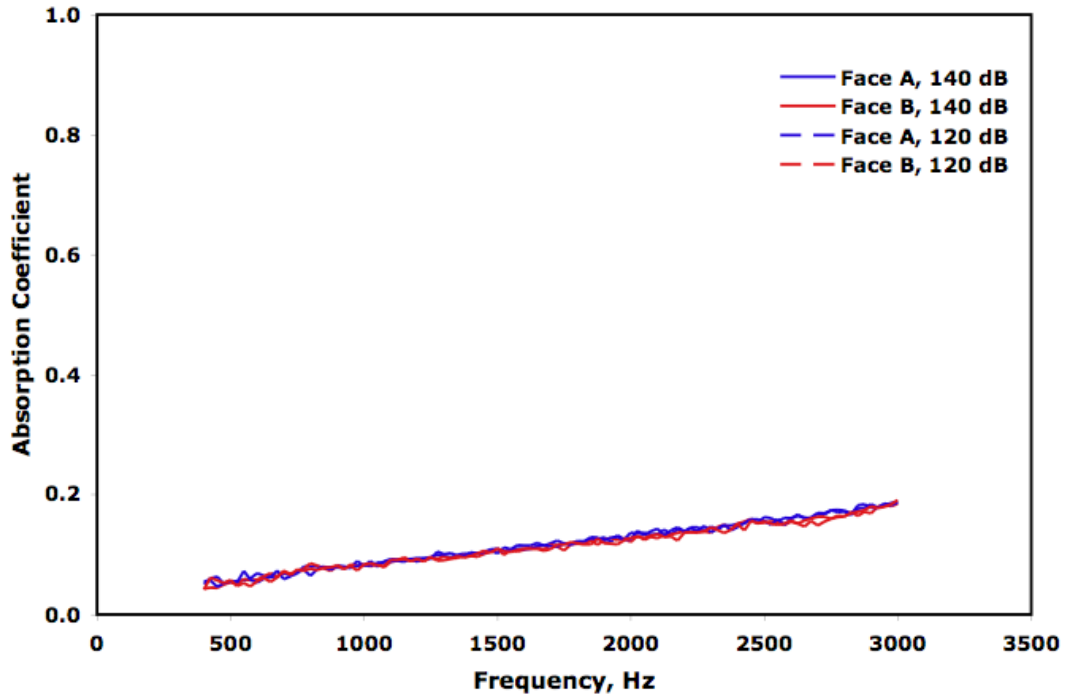
Sample H08

<u>ID</u>	<u>Face A</u>	<u>Face B</u>	<u>Thickness</u>
H08	Tip Rub	Wire EDM	20.7



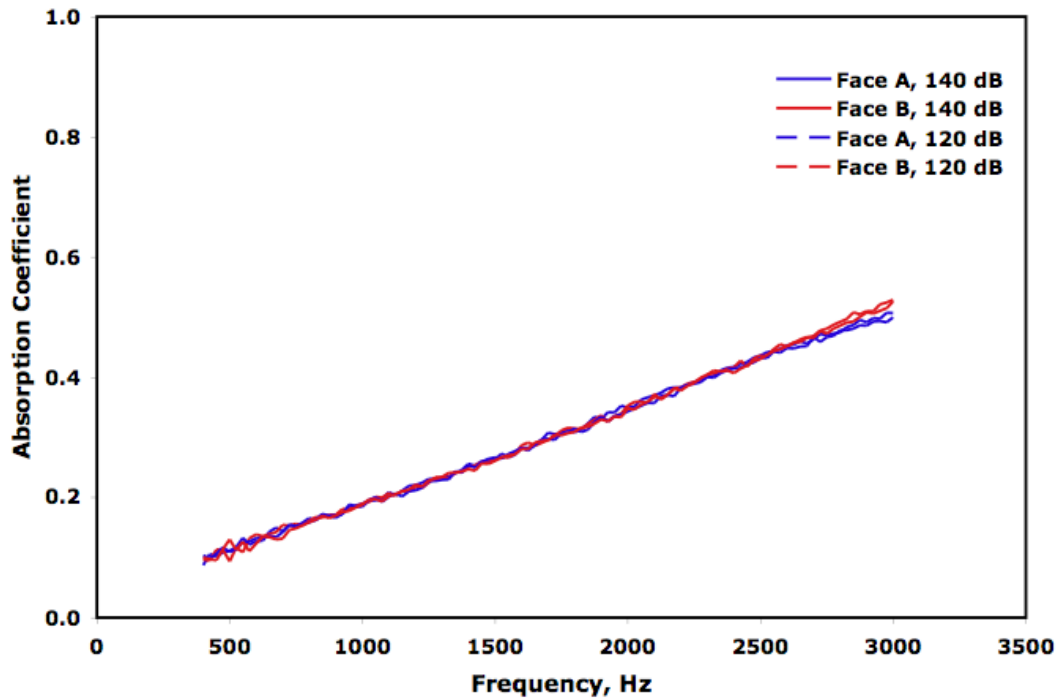
Sample H09

<u>ID</u>	<u>Face A</u>	<u>Face B</u>	<u>Thickness</u>
H09	Tip Rub	Wire EDM	10.1



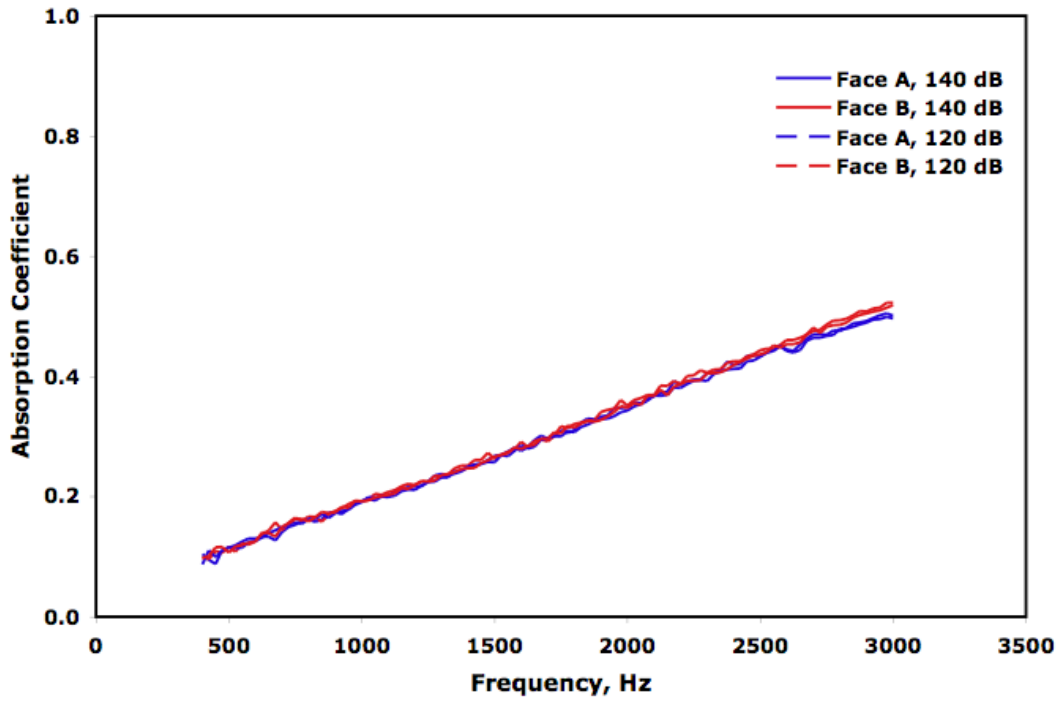
Sample H10

<u>ID</u>	<u>Face A</u>	<u>Face B</u>	<u>Thickness</u>
H10	Wire EDM	As-Received	20.3



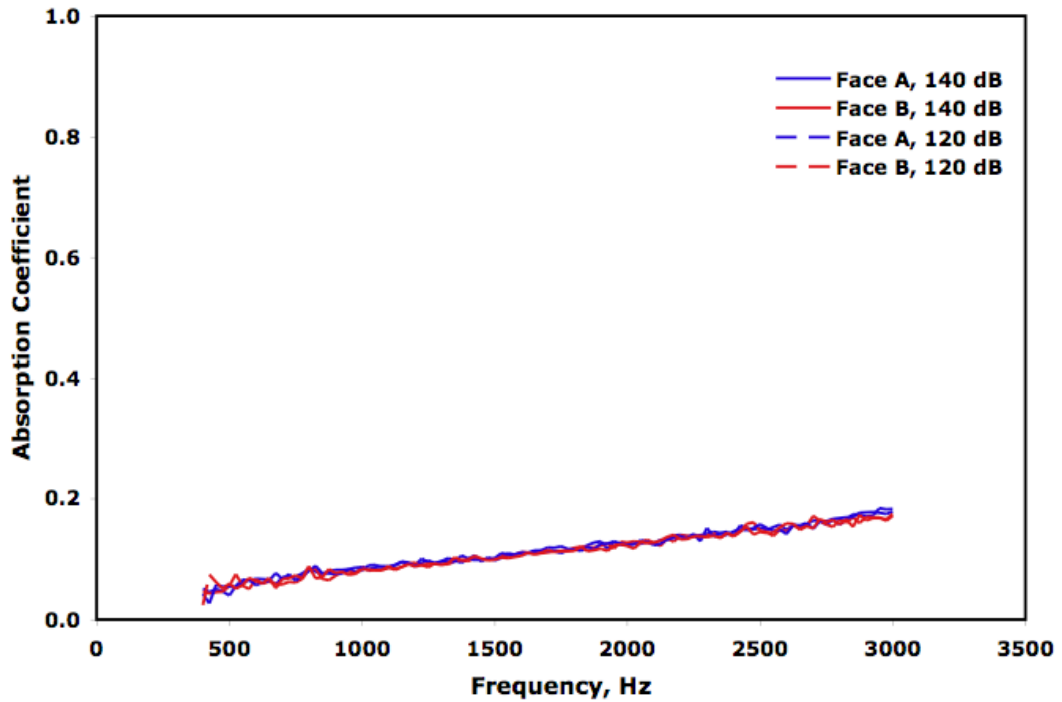
Sample H11

<u>ID</u>	<u>Face A</u>	<u>Face B</u>	<u>Thickness</u>
H11	Wire EDM	As-Received	20.9



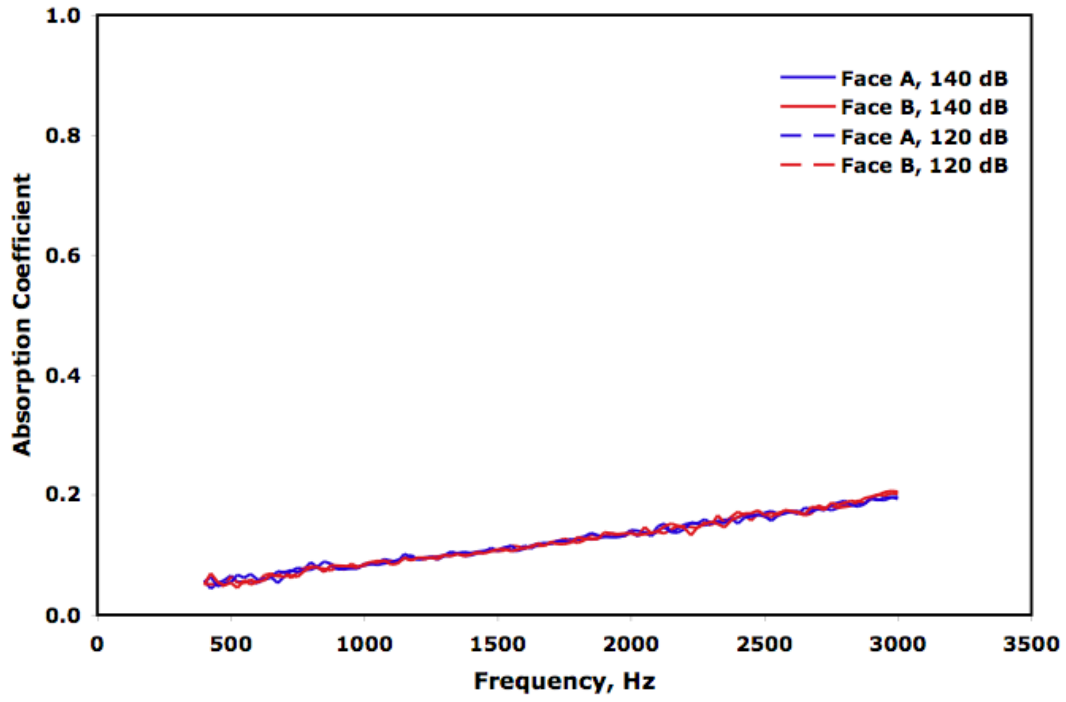
Sample H12

<u>ID</u>	<u>Face A</u>	<u>Face B</u>	<u>Thickness</u>
H12	Wire EDM	Wire EDM	10.1



Sample H13

<u>ID</u>	<u>Face A</u>	<u>Face B</u>	<u>Thickness</u>
H01	Wire EDM	Wire EDM	10.6



REPORT DOCUMENTATION PAGE			Form Approved OMB No. 0704-0188		
<p>The public reporting burden for this collection of information is estimated to average 1 hour per response, including the time for reviewing instructions, searching existing data sources, gathering and maintaining the data needed, and completing and reviewing the collection of information. Send comments regarding this burden estimate or any other aspect of this collection of information, including suggestions for reducing this burden, to Department of Defense, Washington Headquarters Services, Directorate for Information Operations and Reports (0704-0188), 1215 Jefferson Davis Highway, Suite 1204, Arlington, VA 22202-4302. Respondents should be aware that notwithstanding any other provision of law, no person shall be subject to any penalty for failing to comply with a collection of information if it does not display a currently valid OMB control number.</p> <p>PLEASE DO NOT RETURN YOUR FORM TO THE ABOVE ADDRESS.</p>					
<b>1. REPORT DATE (DD-MM-YYYY)</b> 01-12-2009		<b>2. REPORT TYPE</b> Technical Memorandum		<b>3. DATES COVERED (From - To)</b>	
<b>4. TITLE AND SUBTITLE</b> Simulated Tip Rub Testing of Low-Density Metal Foam			<b>5a. CONTRACT NUMBER</b>		
			<b>5b. GRANT NUMBER</b>		
			<b>5c. PROGRAM ELEMENT NUMBER</b>		
<b>6. AUTHOR(S)</b> Bowman, Cheryl, L.; Jones, Michael, G.			<b>5d. PROJECT NUMBER</b>		
			<b>5e. TASK NUMBER</b>		
			<b>5f. WORK UNIT NUMBER</b> WBS 561581.02.08.03.15.03		
<b>7. PERFORMING ORGANIZATION NAME(S) AND ADDRESS(ES)</b> National Aeronautics and Space Administration John H. Glenn Research Center at Lewis Field Cleveland, Ohio 44135-3191			<b>8. PERFORMING ORGANIZATION REPORT NUMBER</b> E-17080		
<b>9. SPONSORING/MONITORING AGENCY NAME(S) AND ADDRESS(ES)</b> National Aeronautics and Space Administration Washington, DC 20546-0001			<b>10. SPONSORING/MONITOR'S ACRONYM(S)</b> NASA		
			<b>11. SPONSORING/MONITORING REPORT NUMBER</b> NASA/TM-2009-215818		
<b>12. DISTRIBUTION/AVAILABILITY STATEMENT</b> Unclassified-Unlimited Subject Categories: 26 and 71 Available electronically at <a href="http://gltrs.grc.nasa.gov">http://gltrs.grc.nasa.gov</a> This publication is available from the NASA Center for AeroSpace Information, 443-757-5802					
<b>13. SUPPLEMENTARY NOTES</b>					
<b>14. ABSTRACT</b> Preliminary acoustic studies have indicated that low-density, open-cell, metal foams may be suitable acoustic liner material for noise suppression in high by-pass engines. Metal foam response under simulated tip rub conditions was studied to assess whether its durability would be sufficient for the foam to serve both as a rub strip above the rotor as well as an acoustic treatment. Samples represented four metal alloys, nominal cell dimensions ranging from 60 to 120 cells per inch (cpi), and relative densities ranging from 3.4 to 10 percent. The resulting rubbed surfaces were relatively smooth and the open cell structure of the foam was not adversely affected. Sample relative density appeared to have significant influence on the forces induced by the rub event. Acoustic responses of various surface preparations were measured using a normal incidence tube. The results of this study indicate that the foam's open-cell structure was retained after rubbing and that the acoustic absorption spectra variation was minimal.					
<b>15. SUBJECT TERMS</b> Metal foams; Porous materials; Abrasion resistance; Acoustic attenuation					
<b>16. SECURITY CLASSIFICATION OF:</b>			<b>17. LIMITATION OF ABSTRACT</b>  UU	<b>18. NUMBER OF PAGES</b> 46	<b>19a. NAME OF RESPONSIBLE PERSON</b> STI Help Desk (email:help@sti.nasa.gov)
<b>a. REPORT</b> U	<b>b. ABSTRACT</b> U	<b>c. THIS PAGE</b> U			<b>19b. TELEPHONE NUMBER (include area code)</b> 443-757-5802



